Marine and Petroleum Geology 145 (2022) 105892

Contents lists available at ScienceDirect

Marine and Petroleum Geology

journal homepage: www.elsevier.com/locate/marpetgeo

Sulfate sources of thermochemical sulfate reduction and hydrogen sulfide distributions in the Permian Changxing and Triassic Feixianguan formations, Sichuan Basin, SW China

Pingping Li [a,b,c,*], Bisong Li [d], Jinbao Duan [d], Yizhen Zhao [b], Huayao Zou [a,b,c], Fang Hao [e]

[a] State Key Laboratory of Petroleum Resources and Prospecting, China University of Petroleum (Beijing), Beijing, 102249, China
[b] College of Geosciences, China University of Petroleum (Beijing), Beijing, 102249, China
[c] Carbonate Research Center, China University of Petroleum (Beijing), Beijing, 102249, China
[d] SINOPEC Exploration Company, Chengdu, Sichuan, 610041, China
[e] China University of Petroleum (East China), Qingdao, Shandong, 266580, China

ARTICLE INFO

Keywords:
Thermochemical sulfate reduction
Hydrogen sulfide
Solid bitumen
Sulfur isotope fractionation
Changxing Formation
Feixianguan Formation
Sichuan Basin

ABSTRACT

The sulfate sources of thermochemical sulfate reduction (TSR) and hydrogen sulfide (H_2S) distributions in the Permian Changxing (P_2c) and Triassic Feixianguan formations (T_1f) in the Sichuan Basin were investigated using geochemical and carbon isotopic data for gases, and sulfur isotopic data for solid bitumen, H_2S, and anhydrite. The concentration of H_2S (>5.0%) is relatively high, and the $\delta^{34}S$ values of the H_2S are significantly higher than those of the Permian source rock kerogen, suggesting a TSR origin for the H_2S. The $\delta^{13}C$ values of the methane and ethane do not increase as the gas souring index ($H_2S/(H_2S+\sum C_n)$) increases, and the $\delta^{34}S$ values of the H_2S are significantly lower than those of the solid bitumen, suggesting mainly liquid hydrocarbon dominated-TSR. The $\delta^{34}S$ values of the solid bitumen and H_2S in the Puguang gas field in the eastern platform are significantly lower than those in the Yuanba gas field in the western platform, and the sulfates for the TSR were most likely derived from the Early and Late T_1f evaporative seawater, respectively. The sulfates required for TSR were most likely enriched during dolomitization based on the positive relationship between the H_2S concentrations and the thickness of the dolostone reservoirs. The H_2S distributions were mainly controlled by the sulfate distributions and the paleo-oil accumulations. The edges of the eastern and western platforms in the Kaijiang-Liangping trough, which were favorable for dolomitization and paleo-oil accumulations, are the most likely H_2S-enriched areas in the Sichuan Basin.

1. Introduction

Thermochemical sulfate reduction (TSR), which can produce toxic and corrosive hydrogen sulfide (H_2S), is a reaction between hydrocarbons and sulfate (Orr, 1974; Machel et al., 1995; Bildstein et al., 2001). Recycling of the H_2S generated by TSR can increase the handling costs of natural gases; however, it also provides valuable sulfur for manufacturing fertilizers, rubber, cosmetics, and pharmaceuticals (Bahadori, 2014). As a result, the initiation conditions, reaction processes, main products, and identification of TSR have been intensively studied through experimental and geological case studies (e.g., Kiyosu and Krouse, 1990; Worden et al., 1995; Heydari, 1997; Hao et al., 2008; Ma et al., 2008a; Cai et al., 2010; Liu et al., 2013, 2014a, b, c; Jenden et al., 2015; Li et al., 2019; Liu et al., 2020).

Sulfate is the main reactant and oxidizing agent in TSR, and its possible sources include seawater, buried seawater, evaporative brine, and/or the dissolution of solid calcium sulfate (Machel et al., 1995). The amount of sulfate can affect the extent of the TSR and the concentration of H_2S generated (Machel, 2001; Hao et al., 2008, 2015; Li et al., 2016). As a result, research on sulfate sources and the spatial distribution of these sulfates can be used to predict the probable spatial distribution of the H_2S (Li et al., 2016), which can reduce the risks associated with oil and gas exploration in H_2S-enriched areas. Correlation between the sulfur isotope ratios ($\delta^{34}S$) of the sulfur-bearing reactant (sulfate) and the sulfur-bearing products (H_2S, solid bitumen, NSO-compounds, elemental sulfur, and pyrite) has commonly been used to determine the sulfate sources for TSR (e.g., Cai et al., 2010; King et al., 2014; Zhu et al., 2005, 2014; Hao et al., 2015; Li et al., 2019). A three-stage TSR

* Corresponding author. State Key Laboratory of Petroleum Resources and Prospecting, China University of Petroleum (Beijing), Beijing, 102249, China.
E-mail address: lpp@cup.edu.cn (P. Li).

https://doi.org/10.1016/j.marpetgeo.2022.105892
Received 15 May 2022; Received in revised form 31 July 2022; Accepted 22 August 2022
Available online 29 August 2022

process (liquid hydrocarbon (oil), wet gas, and methane-dominated TSR) was proposed by Hao et al. (2008), and the sulfur-bearing products were different in each TSR stage (R1, R2, and R3). The main sulfur-bearing products of the liquid hydrocarbon-dominated TSR include NSO-compounds, solid bitumen, and H_2S (R1); those of the wet gas-dominated TSR include H_2S and elemental sulfur (R2); and that of the methane-dominated TSR mainly includes H_2S (R3). The elemental sulfur produced by the wet gas-dominated TSR is unstable and can react with methane to form H_2S if there is sufficient dissolved sulfate (Machel et al., 1995). In addition, the NSO-compounds usually reside in the solid bitumen (Hao et al., 2015). Therefore, the main sulfur-bearing products of TSR should be H_2S and solid bitumen (including NSO-compounds). The $\delta^{34}S$ values of the sulfur-bearing products are lower than those of the sulfate and the sulfur isotope fractionation is mainly controlled by the reaction temperature (Kiyosu and Krouse, 1990). As the TSR continuously progresses, the $\delta^{34}S$ values of the sulfur-bearing products gradually approach the $\delta^{34}S$ values of the sulfate (Machel et al., 1995; Hao et al., 2015). This sulfur isotope fractionation between the sulfate and sulfur-bearing products can be used to determine the sulfate sources for TSR (Zhu et al., 2005; Cai et al., 2010; King et al., 2014; Li et al., 2019).

$$\text{Liquid hydrocarbons} + SO_4^{2-} \rightarrow \text{NSO-compounds} + \text{bitumen} + H_2S + CO_2 \quad \text{(R1)}$$

$$nCaSO_4 + C_nH_{2n+2} \rightarrow nCaCO_3 + H_2S + (n\text{-}1)\ S + nH_2O \quad \text{(R2)}$$

$$CH_4 + CaSO_4 \rightarrow CaCO_3 + H_2S + H_2O \quad \text{(R3)}$$

The natural gas in the Upper Permian Changxing (P_2c) and Lower Triassic Feixianguan (T_1f) formations in the northern and eastern parts of the Sichuan Basin is enriched in H_2S (mainly 0–20.0%, but some of the gas samples from the gas-water transition zone have H_2S contents of up to 60%; Li et al., 2005; Zhu et al., 2005; Hao et al., 2008; Liu et al., 2013, 2014b, c; Li et al., 2015; Wu et al., 2019). The H_2S-enriched gas fields are mainly located in the eastern and western platforms in the Kaijiang-Liangping (K-L) trough. The Puguang (PG), Dukouhe (DKH), and Luojiazhai (LJZ) gas fields are located in the eastern platform, while the Yuanba (YB), Longgang (LG), Xinglongchang (XLC), and Jiannan (JN) gas fields are situated in the western platform (Fig. 1). The H_2S in these gas fields has been confirmed to have a TSR origin, which is supported by the following evidence: the H_2S concentration is high (generally >5.0%), the H_2S and CO_2 concentrations are positively correlated, and the $\delta^{34}S$ values of the H_2S and the sulfur-rich solid bitumen are significantly heavier than those of the Permian source rock kerogen (Li et al., 2005, 2019; Zhu et al., 2005; Cai et al., 2017; Wu et al., 2019). Based on the sulfur isotope correlation between the anhydrite and H_2S, it has been suggested that the sulfate in P_2c-T_1f TSR in the eastern platform was mainly derived from the coeval T_1f anhydrite layers or evaporative brine (Li et al., 2005; Zhu et al., 2014). Based on the correlation between the sulfur isotopes of the solid bitumen and anhydrite in the PG and YB gas fields, Li et al. (2019) determined that the sulfate sources for TSR in the eastern and western platforms differ, and these sources originated from the anhydrite layers or evaporative brine in the Early and Late T_1f, respectively. Zhu et al. (2014) found that the sulfur isotope fractionation between the anhydrite and H_2S in marine strata in the Sichuan Basin is similar (~10.0‰), but they did not conduct a detailed comparison of the $\delta^{34}S$ values of the H_2S in the

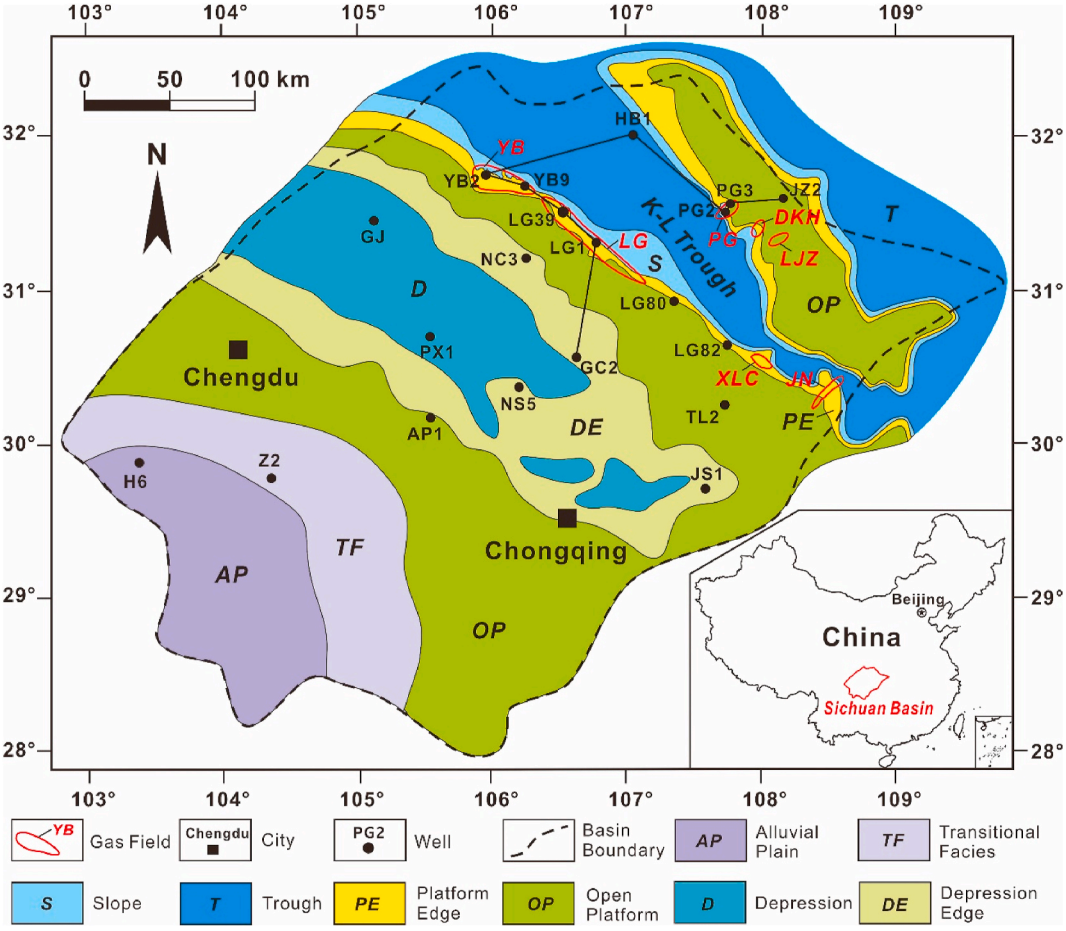

Fig. 1. Locations of the main gas fields, key wells, and sedimentary facies of the Upper Permian Changxing Formation (P_2c) in the Sichuan Basin (modified from Du et al., 2010 and Shu, 2014). YB = Yuanba, LG = Longgang, XLC = Xilongchang, JN = Jiannan, PG = Puguang, LJZ = Luojiazhai, DKH = Dukouhe.

eastern and western platforms. No systematic comparative study of the $\delta^{34}S$ values of the anhydrite, solid bitumen, or H_2S of P_2c-T_1f in the eastern and western platforms has been conducted to corelate the sulfur isotope fractionation or differences in the sulfate sources for TSR. In addition, the gas fields with high H_2S concentrations are mainly located in dolostone reservoirs (Li et al., 2016), but the relationship between the dolomitization process and of the controls of the sulfate sources for TSR remain unclear. Finally, although the H_2S distribution in the eastern platform has been widely studied (e.g., Li et al., 2005; Zhu et al., 2005; Hao et al., 2008; Liu et al., 2013, 2014b; Zhu et al., 2014), the H_2S distribution in the western platform has not yet been carefully studied.

Therefore, the purpose of this study was to determine the sulfate sources for TSR and to predict the H_2S distribution in P_2c and T_1f in the Sichuan Basin based on detailed sulfur isotope correlations between the sulfate, solid bitumen, and H_2S in the PG gas field in the eastern platform and the YB gas field in the western platform. The results of this study

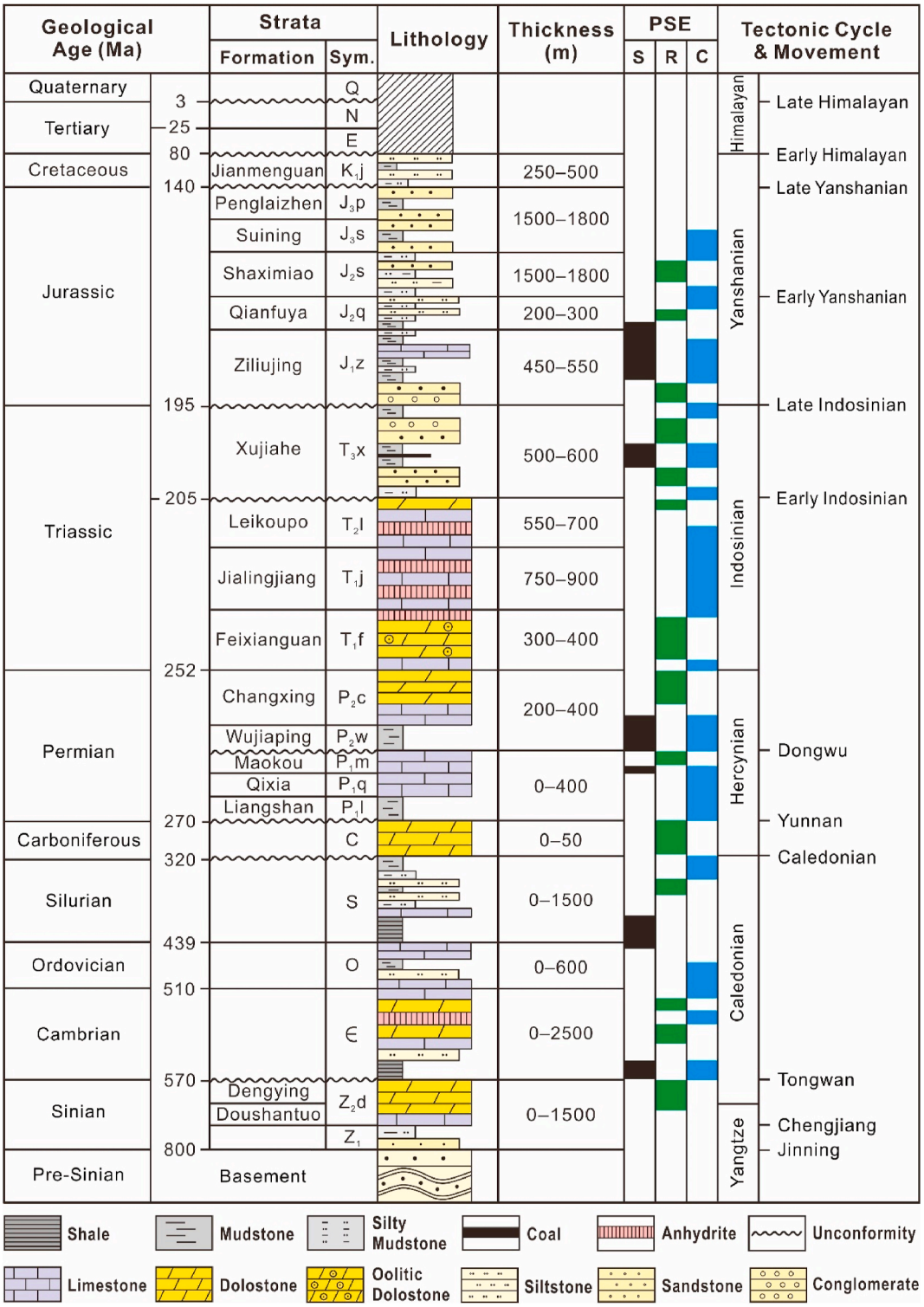

Fig. 2. General stratigraphy, lithology, tectonic cycles and movements in the Sichuan Basin (modified from Zhai, 1989). Sym. = symbol, PSE = petroleum system element, S = source rock, R = reservoir, C = caprock.

provide an important reference for natural gas exploration in P_2c and T_1f in the western platform in the K-L trough. It is also a useful geological case study of sulfur isotope fractionation during TSR, which improves prediction of the H_2S distributions in deep marine carbonate reservoirs.

2. Geologic setting

The Sichuan Basin in southwestern China, is one of the main natural gas production basements in China (Fig. 1). Since the formation of the pre-Sinian basement, the Sichuan Basin has experienced six tectonic cycles and movements (including the Yangtze, Caledonian, Hercynian, Indosinian, Yanshanian, and Himalayan movements; Zhai, 1989), and it contains Sinian to Cretaceous strata with a total thickness of about 6000–12,000 m (Fig. 2). The Yangtze, Caledonian, Hercynian, and Early Indosinian movements were characterized by subsidence and uplift and by deposition of marine carbonates and shale; while the Late Indosinian, Yanshanian, and Himalayan movements were characterized by lateral compression and uplift and by deposition of continental shale, sandstone, and conglomerate (Zhai, 1989; Ma et al., 2007; Liu et al., 2021).

After the Late Carboniferous uplift and erosion in the Sichuan Basin, a transgression event began in the Early Permian (Huang et al., 2017). The Liangshan Formation was deposited in a transitional environment and is composed of shale and siltstone; while the subsequent Qixia and Maokou formations were deposited in an open platform environment and are mainly composed of micritic limestone and bioclastic limestone. At the end of the deposition of the Maokou Formation, a large-scale basaltic eruption occurred in the southwestern Sichuan Basin (260–257 Ma; Shellnutt, 2014) and northwest-southeast trending subsidence occurred in the northern and eastern Sichuan Basin (Wang et al., 2021). Then, the marine shale and mudstone of the Wujiaping Formation (P_2w) were deposited in this subsidence area. During the deposition of the Upper Permian Changxing Formation (P_2c), the K-L trough (Wang et al., 2001) formed in the previous subsidence area (Fig. 1). An isolated platform and a large platform adjacent to the continent were developed in the eastern and western parts of the K-L trough, respectively. Reefs and bioclastic shoals, mainly composed of dolostone, developed on the edges of both the eastern and western platforms, while micritic limestone and shale were deposited in the slope and trough areas. This platform-trough framework persisted during the deposition of the Lower Triassic Feixianguan Formation (T_1f). The T_1f can be further divided into four members (T_1f^1, T_1f^2, T_1f^3, and T_1f^4) from bottom to top. During the deposition of the Early T_1f (T_1f^1 and T_1f^2), oolitic shoals developed on the platform edges and an evaporative platform developed on the eastern isolated platform (Ma et al., 2007; Du et al., 2010). During the deposition of the Late T_1f ($T_1f^3$and T_1f^4), the K-L trough was completely filled. At the end of T_1f^4, a large restricted and evaporitic platform, consisting of limestone and anhydrite, formed in the northern and eastern Sichuan Basin. Subsequently, the Lower Triassic Jialingjiang (T_1j) and Middle Triassic Leikoupo (T_2l) formations, consisting of limestone and anhydrite, were deposited on the previously formed restricted and evaporitic platforms (Zhai, 1989).

Many medium to large gas fields have been discovered in edges of both the eastern and western platforms in the K-L trough (Fig. 1) (Ma et al., 2007; Du et al., 2010; Guo et al., 2018). The P_2c and T_1f dolostones of the reefs and shoals on the platform edges are the main reservoirs, and the anhydrite layers and dense limestone of the Late T_1f and the overlying T_1j are the main caprocks (Ma et al., 2008b). As shown in Fig. 3, P_2c and T_1f^{1-3} are the gas reservoirs in the PG gas field, and P_2c and T_1f^2 are the gas reservoirs in the YB gas field. The hydrocarbon gases in these gas fields were mainly formed via oil-cracking and were altered by TSR (Hao et al., 2008; Li et al., 2015; Liu et al., 2013; Wu et al., 2019), and they were mainly derived from the Upper Permian source rocks (Li et al., 2005; Zou et al., 2008; Wu et al., 2019). The maximum burial temperature of the gas reservoirs exceeded 200 °C, and the Upper Permian source rocks exhibit high organic maturity, with vitrinite reflectance (R_o) values of greater than 2.0% in the PG and YB gas fields (Fig. 3) (Hao et al., 2008; Li et al., 2015).

3. Sampling and analytical methods

Fifteen P_2c natural gas samples were collected from gas production wells in the YB gas field. The chemical and isotopic compositions (including the $\delta^{13}C$ of the methane, ethane, and CO_2) of these gas samples were analyzed in the Geochemical Analysis and Testing Center of the Northwest Institute of Eco-Environment and Resources (Chinese Academy of Sciences), using a Finnigan MAT-271 mass spectrometer and a Finnigan MAT-253 instrument, respectively. The detailed analytical procedures used to analyze the gas samples have been described by Liu et al. (2013). The H_2S of these natural gas samples was precipitated as Ag_2S using an oversaturated silver nitrate solution.

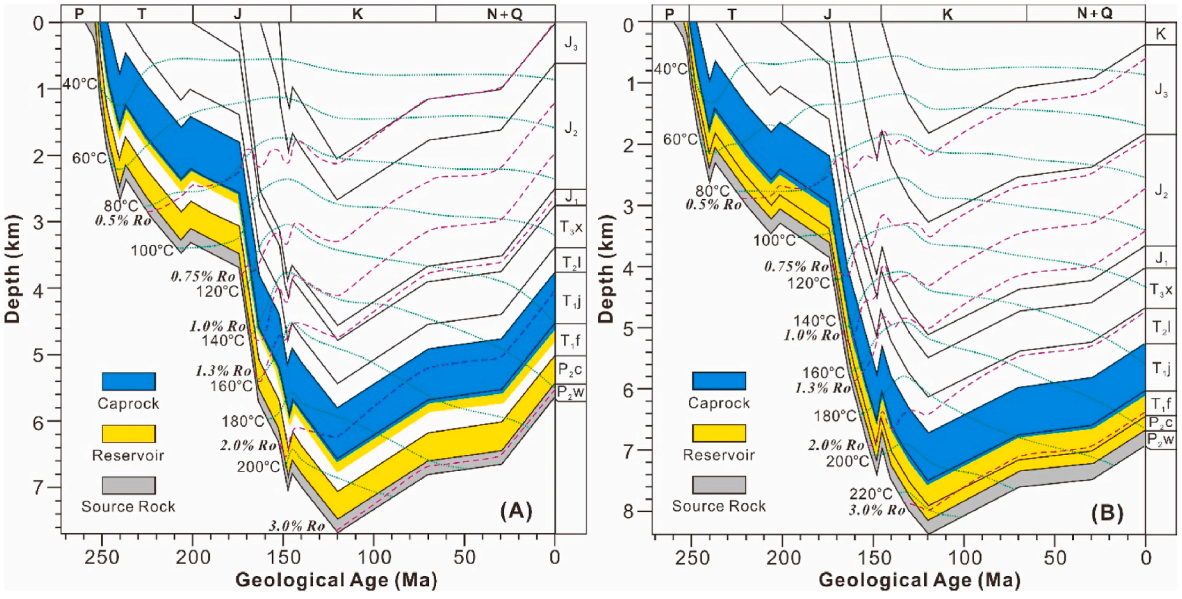

Fig. 3. General burial and thermal history of the Permian source rocks and gas reservoirs in the (A) Puguang and (B) Yuanba gas fields (modified from Hao et al., 2008 and Li et al., 2015). *Ro* = equivalent vitrinite reflectance. Note: the *Ro* values were calculated using the EASY%Ro model (Sweeney and Burnham, 1990), and the burial history was obtained using the PetroMod 11 software.

Finally, the Ag_2S precipitate was combusted in a Thermo EA Flash 2000 at 1000 °C, and the sulfur isotopes ($\delta^{34}S$) were determined using a Delta V Plus mass spectrometer calibrated using International Atomic Energy Agency (IAEA) standards at the State Key Laboratory of Biogeology and Environmental Geology (China University of Geosciences, Wuhan). The results are reported as $\delta^{34}S$ relative to the Vienna Canyon Diablo Troilite (VCDT) standard, and the average precision of the analyses based on replicate analyses of the IAEA standards is ±0.3‰.

In addition, the chemical and carbon isotopic compositions of the gases from the YB and PG gas fields, and the $\delta^{34}S$ values of the H_2S, solid bitumen and anhydrite in the NE Sichuan Basin were also collected from published papers (Wang et al., 2002; Zhu et al., 2005, 2008; Ma et al., 2008b; Hao et al., 2008; Zheng et al., 2009; Cai et al., 2010, 2017; Li et al., 2015, 2019).

4. Results

The chemical compositions, carbon isotopic compositions ($\delta^{13}C$) of the hydrocarbon gases (methane and ethane) and CO_2, and the sulfur isotopes ($\delta^{34}S$) of the H_2S of the 15 P_2c natural gas samples from the YB gas field are presented in Table 1. The P_2c natural gases are dominated by hydrocarbon gases (>80.0%), which are mainly composed of methane (82.92%–91.47%) and ethane (0.03%–0.05%); and the gas dryness ($C_1/\sum C_n$) is generally greater than 99.95%. In addition, the non-hydrocarbon gases mainly included H_2S (3.02%–9.79%), CO_2 (3.14%–6.79%), and nitrogen (N_2, 0.06%–0.69%). The gas souring index (GSI = $H_2S/(H_2S+\sum C_n)$; Worden et al., 1995), which indicates the extent of the TSR, is between 0.03 and 0.11. The $\delta^{13}C$ values of the methane, ethane, and CO_2 range from −30.3‰ to −26.4‰, −27.9‰ to −24.9‰, and −1.6‰ to +2.8‰, respectively; and the $\delta^{34}S$ values of the H_2S range from 19.7‰ to 25.6‰.

5. Discussion

5.1. Multiple lines of evidence for a TSR origin of the H_2S

There are three main causes of H_2S in hydrocarbon reservoirs: bacterial sulfate reduction (BSR), thermal decomposition of the organic sulfur compounds in kerogen or oil (TDS), and TSR (Orr, 1977; Worden et al., 1995; Machel, 2001). H_2S of different origins has different concentrations and sulfur isotope compositions. BSR mainly occurs in low temperature environments (<80 °C; Orr, 1977; Machel, 1987). Moreover, the concentration of the H_2S produced via BSR is generally less than 5%, and the sulfur isotope fractionation between the sulfate and H_2S is relatively large (15‰–65‰; Machel et al., 1995). The concentration of H_2S produced by TDS is relatively low (<5.0%), and the $\delta^{34}S$ values of the H_2S are close to the $\delta^{34}S$ values of the source rock kerogen (Orr, 1977, 1986; Idiz et al., 1990; Amrani et al., 2005; Rosenberg et al., 2017). TSR occurs in relatively high temperature environments (>100–120 °C; Orr, 1974; Worden et al., 1995), and the concentration of H_2S gradually increases as TSR progresses and can be relatively high (>5.0%) (Amrani et al., 2005; Rosenberg et al., 2017). In addition, the $\delta^{34}S$ values of the H_2S are much lower than the $\delta^{34}S$ values of sulfate in the initial stage of TSR, but $\delta^{34}S$ values of the H_2S are close to the $\delta^{34}S$ values of the sulfate in the late stage of TSR (Amrani et al., 2005; Meshoulam et al., 2016; Rosenberg et al., 2017) and are significantly heavier than the $\delta^{34}S$ values of the source rock kerogen (Machel et al., 1995; Cai et al., 2017) because more ^{34}S from the sulfate is transformed into H_2S as the TSR progresses.

The relatively high H_2S concentrations of the P_2c gases from the YB gas field (mainly between 2.0% and 10.0%; Fig. 4A) and those of the T_1f-P_2c gases from the PG gas field (mainly between 10.0% and 18.0%; Fig. 4A) suggest that the H_2S in these two gas fields was most likely produced by TSR rather than by BSR or TDS (<5.0%). The rough positive relationships between the H_2S and CO_2 concentrations and between the CO_2 concentrations and GSI values of the natural gases in the PG and YB gas fields (Fig. 4A and B) also support a TSR origin for the H_2S (Worden et al., 1995). As the GSI increases, the gas dryness ($C_1/\sum C_n$) becomes relatively high (99.8%–100%; Fig. 4C) and the total hydrocarbon gas concentration ($\sum C_n$) decreases linearly ($R^2 = 0.80$; Fig. 4D), suggesting the consumption of the heavy hydrocarbon gases during TSR. The differences between the $\delta^{13}C$ values of the methane and ethane ($\delta^{13}C_1-\delta^{13}C_2$) in most of the gas samples are below zero ($\delta^{13}C_1<\delta^{13}C_2$; Fig. 5C), also suggesting a transition from reversed carbon isotope ratios ($\delta^{13}C_1>\delta^{13}C_2$) to normal carbon isotope ratios ($\delta^{13}C_1<\delta^{13}C_2$) due to TSR (Hao et al., 2008; Liu et al., 2013, 2019, 2020). In addition, the relatively high concentrations of CO_2 (>3.0%) and the heavy $\delta^{13}C$ values of the CO_2 (−3.0‰ to +3.0‰; Fig. 5D) suggest that the CO_2 was the combined result of TSR and subsequent re-equilibrium with the ^{13}C-enriched water-rock system (Liu et al., 2014a).

The atomic S/C ratios of the P_2c solid bitumen in the YB gas fields and the T_1f-P_2c solid bitumen in the PG gas fields are 0.03–0.14 and 0.06–0.08, respectively (Hao et al., 2015; Li et al., 2016). Solid bitumen with atomic S/C ratios of greater than 0.03 is considered to be of TSR origin (Kelemen et al., 2008). In addition, the $\delta^{34}S$ values of the solid bitumen (24.1‰–34.2‰; Li et al., 2019) are significantly heavier than the $\delta^{34}S$ values of the Permian source rock kerogen (−6.6‰–4.1‰, average of 1.3‰); Cai et al. (2010), 2017). The difference between the $\delta^{34}S$ values of the kerogen and solid bitumen is small (within 2.0‰; Idiz et al., 1990; Amrani et al., 2005). As a result, the sulfur-enriched solid bitumen with heavy sulfur isotopes in the YB and PG gas fields is completely different from the solid bitumen of TDS origin. The $\delta^{34}S$ values of the H_2S in the YB (19.7‰–25.6‰) and PG gas fields (10.0–14.0‰; Zhu et al., 2005; Ma et al., 2008b) are also significantly heavier than those of the Permian source rock kerogen, and they are close to the $\delta^{34}S$ values of the Late T_1f anhydrite (average of 34.6‰; Li et al., 2019) and Early T_1f anhydrite (average of 22.7‰; Wang et al., 2002; Zhu et al., 2005), which were probably the sulfate sources of the TSR in the two gas fields (discussed in next section). This further supports the conclusion that the H_2S in the YB and PG gas fields was not produced via TDS but has a TSR origin. Finally, the average sulfur isotope fractionation between the sulfate and H_2S is 10.6‰ and 12.1‰ in the YB and PG gas fields, respectively (Fig. 6), which is much smaller than the sulfur isotope fractionation produced by BSR (15–65‰; Machel et al., 1995). These facts rule out the possibility that the H_2S was produced via BSR and supports a TSR origin for the H_2S in the YB and PG gas fields.

Solid bitumen is commonly found in the P_2c reservoir in the YB and PG gas fields, and the hydrocarbon gases are mainly secondary oil-cracking gases (Hao et al., 2008; Li et al., 2015). In addition, anhydrite layers developed in the Early and Late T_1f adjacent to the T_1f-P_2c gas reservoir in the PG and YB gas fields, respectively. This means that the main reactants (hydrocarbons and sulfate) for TSR occur in these two gas fields. Finally, the maximum burial temperature of the T_1f-P_2c reservoir in the YB and PG gas fields exceeded 200 °C (Fig. 3), which is much higher than the onset temperature for the initiation of TSR (about 100–120 °C; Worden et al., 1995). This indicate that the main reactants and the external temperature conditions required for TSR were present in the YB and PG gas fields, which further supports a TSR origin for the H_2S in these two gas fields.

In summary, the relatively high H_2S concentrations and heavy sulfur isotope ratios ($\delta^{34}S$) of the solid bitumen and H_2S (close to the $\delta^{34}S$ of the probable sulfate source) provide adequate evidence to support a TSR origin for the H_2S in the YB and PG gas fields. In addition, that replacement of previously formed anhydrite by calcite and the light $\delta^{13}C$ values of the post-bitumen calcite, which were suggested have a TSR origin in the southeastern Mississippi salt basin (Heydari and Moore, 1989), has been reported in the PG and YB gas fields (Zhang, 2009; Li et al., 2015). This further supports a TSR origin for the H_2S in the two gas fields.

Table 1
Chemical and isotopic compositions of T_1f and P_2c natural gases from the Yuanba and Puguang gas fields in the Sichuan Basin.

Gas field	Well	Strata	Depth (m)	Chemical Composition (%)					C_1/C_{1-3}%	GSI	$\delta^{13}C$ (PDB, ‰)			$\delta^{34}S$ (‰)	Data Source
				CH_4	C_2H_6	H_2S	CO_2	N_2			CH_4	C_2H_6	CO_2	H_2S	
Yuanba	YB10–1H	P_2c	7215–7749	84.64	0.04	8.24	6.79	0.28	99.95	0.09	−30.3	−26.8	−1.3	22.8	This study
Yuanba	YB10–C1	P_2c	7011–7180	83.09	0.04	9.77	6.71	0.38	99.95	0.11	−26.9	−27.2	2.2	23.6	This study
Yuanba	YB103H	P_2c	7047–7696	83.42	0.04	9.44	6.77	0.32	99.95	0.10	−27.4	−27.9	2.3	21.7	This study
Yuanba	YB27–1H	P_2c	6315–7468	89.50	0.03	6.66	3.14	0.65	99.96	0.07	−26.7	−25.9	0.1	20.1	This study
Yuanba	YB29	P_2c	6636–6698	87.31	0.04	6.99	5.32	0.34	99.96	0.07	−26.9	−25.2	2.2	24.7	This study
Yuanba	YB29–2H	P_2c	6994–7686	87.42	0.04	6.47	5.64	0.44	99.96	0.07	−28.1	−26.1	1.2	23.7	This study
Yuanba	YB101–1H	P_2c	6969–7950	82.92	0.03	9.79	7.19	0.06	99.96	0.11	−28.6	−27.8	−0.1	25.6	This study
Yuanba	YB102–2H	P_2c	7100–7500	87.68	0.04	6.43	5.47	0.37	99.95	0.07	−27.5	−26.5	2.8	23.4	This study
Yuanba	YB103–1H	P_2c	6883–7508	83.71	0.04	9.23	6.70	0.32	99.95	0.10	−28.9	−27.5	1.5	22.3	This study
Yuanba	YB104	P_2c	6700–6750	85.45	0.05	8.19	5.92	0.39	99.95	0.09	−28.4	−27.2	−0.6	21.5	This study
Yuanba	YB204-2	P_2c	6511–6650	91.47	0.05	3.02	5.33	0.13	99.95	0.03	−27.6	−24.9	2.0	23.8	This study
Yuanba	YB205	P_2c	6448–6711	87.67	0.04	6.06	5.86	0.36	99.95	0.06	−27.2	−26.3	1.4	23.3	This study
Yuanba	YB271	P_2c	6320–6370	88.92	0.04	7.17	3.19	0.68	99.96	0.07	−27.0	−25.0	−1.6	20.5	This study
Yuanba	YB272H	P_2c	6636–6699	88.49	0.04	7.42	3.36	0.69	99.96	0.08	−26.4	−25.5	1.3	19.7	This study
Yuanba	YB273	P_2c	6806–6915	87.88	0.04	7.43	4.35	0.29	99.96	0.08	−30.3	−26.0	0.6	20.6	This study
Yuanba	YB1–C1	P_2c	7331–7368	86.72	0.04	6.61	6.25	0.28	99.95	0.07	ND	ND	ND	ND	Li et al. (2015)
Yuanba	YB10–C1	P_2c	7011–7180	86.16	0.04	7.25	6.24	0.28	99.95	0.08	ND	ND	ND	ND	Li et al. (2015)
Yuanba	YB101	P_2c	6955–7022	81.51	0.08	7.15	1.63	4.51	99.90	0.08	−31	ND	−1.7	ND	Li et al. (2015)
Yuanba	YB102	P_2c	6711–6791	84.33	0.05	4.36	9.72	1.45	99.94	0.05	−29.4	ND	ND	ND	Li et al. (2015)
Yuanba	YB103H	P_2c	7047–7696	85.18	0.04	7.11	6.06	0.24	99.95	0.08	ND	ND	ND	ND	Li et al. (2015)
Yuanba	YB104	P_2c	6700–6726	87.09	0.04	7.04	5.23	0.52	99.95	0.07	−29.1	−25.6	−0.77	ND	Li et al. (2015)
Yuanba	YB107	P_2c	6676–6694	90.83	0.05	3.30	5.38	0.37	99.94	0.04	ND	ND	ND	ND	Li et al. (2015)
Yuanba	YB11	P_2c	6797–6917	82.16	0.06	6.18	11.31	0.25	99.93	0.07	ND	ND	ND	ND	Li et al. (2015)
Yuanba	YB12	P_2c	6692–6780	77.68	0.04	9.84	3.68	2.72	99.95	0.11	−30	ND	−0.7	ND	Li et al. (2015)
Yuanba	YB123	P_2c	6904–6918	78.04	0.04	8.96	11.02	1.90	99.95	0.10	−29.3	−29.9	−1.3	ND	Li et al. (2015)
Yuanba	YB124–C1	P_2c	6940–7483	80.64	0.04	9.90	7.26	0.01	99.95	0.11	ND	ND	ND	ND	Li et al. (2015)
Yuanba	YB16	P_2c	6950–6974	84.58	0.23	12.16	2.56	0.46	99.73	0.13	−29.7	ND	−1.3	ND	Li et al. (2015)
Yuanba	YB2	P_2c	6677–6700	83.21	0.06	4.37	10.95	1.36	99.93	0.05	ND	ND	ND	ND	Li et al. (2015)
Yuanba	YB2	P_2c	6545–6593	85.56	0.13	3.81	8.78	1.40	99.85	0.04	−30.5	ND	−2.3	ND	Li et al. (2015)
Yuanba	YB204	P_2c	6523–6590	91.23	0.04	2.36	4.32	1.54	99.96	0.03	−29.4	−26	−1.4	ND	Li et al. (2015)
Yuanba	YB205	P_2c	6698–6711	89.56	0.04	4.97	4.79	0.59	99.96	0.05	−27.9	ND	−0.86	ND	Li et al. (2015)
Yuanba	YB205	P_2c	6448–6480	89.14	0.05	5.33	5.03	0.00	99.94	0.06	−29.5	−27.5	−1.2	ND	Li et al. (2015)
Yuanba	YB27	P_2c	6262–6319	89.03	0.09	4.08	5.06	1.22	99.90	0.04	−28.9	−26.6	−1.2	ND	Li et al. (2015)
Yuanba	YB28	P_2c	6796–6817	88.12	0.01	5.49	5.44	0.85	99.99	0.06	ND	ND	ND	ND	Li et al. (2015)
Yuanba	YB29	P_2c	6808–6820	88.76	0.06	1.20	7.03	4.02	99.93	0.01	−28.9	−29.3	−3	ND	Li et al. (2015)
Yuanba	YB271	P_2c	6320–6370	90.39	0.04	5.20	3.28	1.01	99.96	0.05	ND	ND	ND	ND	Li et al. (2015)
Yuanba	YB273	P_2c	6811–6880	89.92	0.04	5.59	3.86	0.53	99.96	0.06	ND	ND	ND	ND	Li et al. (2015)
Yuanba	YB224	P_2c	6625–6636	84.76	0.06	10.61	4.08	0.34	99.93	0.11	ND	ND	ND	ND	Li et al. (2015)
Puguang	PG1	T_1f	5602–5668	77.81	0.03	12.44	9.07	0.61	99.96	0.14	−31.06	−25.04	ND	ND	Hao et al. (2008)
Puguang	PG2	T_1f	4775–4826	76.69	0.19	14.80	7.89	0.40	99.75	0.16	−30.93	−28.51	1.89	ND	Hao et al. (2008)
Puguang	PG2	T_1f	4934–4985	74.46	0.22	16.89	7.89	0.51	99.71	0.18	−30.49	−29.07	ND	ND	Hao et al. (2008)
Puguang	PG2	T_1f	5007–5102	75.63	0.11	15.82	7.96	0.44	99.85	0.17	−30.96	−28.81	ND	ND	Hao et al. (2008)
Puguang	PG2	P_2c	5237–5282	75.07	0.24	15.66	8.57	0.43	99.68	0.17	−30.05	−27.67	ND	ND	Hao et al. (2008)
Puguang	PG3	T_1f	5262–5349	71.16	0.02	9.27	18.03	0.55	99.97	0.12	−29.71	ND	−7.86	ND	

(*continued on next page*)

Table 1 (*continued*)

Gas field	Well	Strata	Depth (m)	Chemical Composition (%)					C_1/C_{1-3}%	GSI	$\delta^{13}C$ (PDB, ‰)			$\delta^{34}S$ (‰)	Data Source
				CH_4	C_2H_6	H_2S	CO_2	N_2			CH_4	C_2H_6	CO_2	H_2S	
															Hao et al. (2008)
Puguang	PG4	T_1f	5759–5791	73.59	0.04	17.41	8.39	0.54	99.95	0.19	ND	ND	ND	ND	Hao et al. (2008)
Puguang	PG5	T_1f	4830–4868	73.51	0.03	11.42	14.25	0.72	99.96	0.13	−33.66	ND	2.41	ND	Li et al. (2015)
Puguang	PG5	P_2c	5141–5243	72.20	0.03	13.52	13.55	0.64	99.96	0.16	ND	ND	ND	ND	Li et al. (2015)
Puguang	PG6	T_1f	4851–4893	75.44	0.03	11.01	12.68	0.80	99.96	0.13	−33.14	ND	1.96	ND	Hao et al. (2008)
Puguang	PG6	T_1f	5030–5158	74.67	0.03	14.05	10.53	0.65	99.96	0.16	−29.49	ND	1.84	ND	Hao et al. (2008)
Puguang	PG6	P_2c	5295–5385	75.92	0.05	14.71	8.74	0.49	99.93	0.16	ND	ND	ND	ND	Hao et al. (2008)
Puguang	PG8	P_2c	5502–5592	83.14	0.04	8.22	7.02	1.50	99.95	0.09	−31.36	ND	1.03	ND	Li et al. (2015)
Puguang	PG8	P_2c	5634–5643	73.39	0.00	14.60	4.42	0.63	100.00	0.17	ND	ND	ND	ND	Li et al. (2015)
Puguang	PG9	T_1f	5739–5852	73.70	0.02	15.70	9.94	0.59	99.97	0.18	−31.04	ND	−0.04	ND	Li et al. (2015)
Puguang	PG9	T_1f	5916–5993	70.31	0.02	16.17	12.52	0.90	99.97	0.19	−31.6	ND	0.42	ND	Li et al. (2015)
Puguang	PG9	P_2c	6110–6130	69.64	0.03	14.57	14.10	1.05	99.96	0.17	−31.31	−23.87	0.94	ND	Li et al. (2015)
Puguang	PG9	P_2c	6151–6175	72.97	0.02	15.36	5.71	5.25	99.97	0.17	−31.03	ND	0.75	ND	Li et al. (2015)
Puguang	PG101	T_1f	5776–5786	76.24	0.41	14.43	8.45	0.38	99.47	0.16	ND	ND	ND	ND	Li et al. (2015)
Puguang	PG2	T_1f	5027	80.02	0.06	14.71	2.55	0.46	99.93	0.16	ND	ND	ND	10.28	Zhu et al. (2005)
Puguang	PG2	T_1f	5200	79.28	0.05	15.67	2.94	2.43	99.94	0.16	ND	ND	ND	12.47	Zhu et al. (2005)
Puguang	PG3	T_1f	5262–5349	66.43	0.02	15.69	16.48	0.52	99.97	0.19	ND	ND	ND	ND	Zhu et al. (2008)
Puguang	PG5	T_1f	4830–4868	73.51	0.03	11.42	14.25	0.72	99.96	0.13	ND	ND	ND	12.72	Zhu et al. (2008)
Puguang	PG6	T_1f	5030–5158	73.9	0.03	14.8	10.69	0.78	99.96	0.17	ND	ND	ND	12.41	Zhu et al. (2008)

5.2. Sulfate sources for the TSR and oil-dominated TSR

The main sulfur-bearing products of TSR include NSO-compounds, solid bitumen, H_2S, elemental sulfur, and metal sulfides (e.g., pyrite) (Machel et al., 1995; Hao et al., 2008, 2015). The NSO-compounds are transferred into solid bitumen (Hao et al., 2015), the elemental sulfur is unstable and continues to react with hydrocarbons to form H_2S (Machel et al., 1995), and the amount of pyrites is usually small because the amount of iron cations in the carbonate reservoir fluid is generally small. Therefore, for most TSR processes in deep reservoirs, the most important sulfur-bearing products should be solid bitumen and H_2S.

The sulfur isotope fractionation between the original sulfate and the sulfur-bearing products (solid bitumen and H_2S) was controlled by the sufficiency of the sulfate and the TSR processes. If the sulfate is limited and all of the sulfur in the dissolved sulfate was consumed and transformed into H_2S during the TSR, there should be no sulfur isotope fractionation between the sulfate and the H_2S produced (Machel et al., 1995); meanwhile, if there is excess sulfate and only part of the sulfur in the sulfate is transformed into H_2S, there should be sulfur isotope fractionation between the reactant (sulfate) and products (solid bitumen and H_2S). In addition, the sulfur isotope fractionation is different in the different TSR processes (Meshoulam et al., 2016). In the initial stage (under relatively low temperatures) of TSR, there is kinetic isotope fractionation which can be characterized by an empirical formula (Kiyosu and Krouse, 1990). The initial S–O bond rupture of the sulfate ions (SO_4^{2-}) is affected by the temperature, and it is easier to break the ^{32}S–O bond than the ^{34}S–O bond (Harrison and Thode, 1957). Consequently, ^{32}S is preferentially incorporated into the H_2S and the ^{34}S preferentially resides in the dissolved sulfate, resulting in sulfur isotope fractionation between the sulfate and H_2S (Kiyosu and Krouse, 1990). The fractionation decreases as the H_2S concentration increases and the reactions enter the catalyzed stage, and the sulfur isotope fractionation between the sulfate and H_2S is small (Meshoulam et al., 2016). As the TSR progresses, more ^{34}S will be used to form H_2S, resulting in the $\delta^{34}S$ values of the sulfur-bearing products gradually approaching the $\delta^{34}S$ values of the sulfate (Hao et al., 2015). Therefore, $\delta^{34}S$ values of the sulfate for TSR can be determined from the $\delta^{34}S$ values of sulfur-bearing products, and then, the possible sulfate sources can be analyzed.

The SO_4^{2-} concentrations of the formation water in the PG and YB gas fields are extremely low (<1.0 g/L; Li et al., 2016), suggesting that the sulfates were basically consumed during the TSR process. Therefore, theoretically, there should be no significant sulfur isotope fractionation between the original sulfates and the TSR products (solid bitumen and H_2S). The $\delta^{34}S$ values of the H_2S in the YB and PG gas fields are 19.7‰–25.6‰ (average of 22.5‰) and 10.3‰–13.7‰ (average of 12.1‰), respectively; while the $\delta^{34}S$ values of the solid bitumen in the YB and PG gas fields are 24.1‰–34.2‰ (average of 27.9‰) and 12.0‰–24.0‰ (average of 17.2‰), respectively (Fig. 6). The $\delta^{34}S$ values of the H_2S and solid bitumen in the YB gas field are greater than those of the H_2S and solid bitumen in the PG gas field (Fig. 6), suggesting that the sulfate sources for TSR may have been different in these two gas fields. In particular, the $\delta^{34}S$ values of the bitumen from the YB gas field are greater than those of the Early T_1f anhydrite and are close to those of the Late T_1f anhydrite, while the $\delta^{34}S$ values of the bitumen from the PG gas field are similar to those of the Early T_1f anhydrite, but is significantly lower than that of the Late T_1f anhydrite (Fig. 6). This indicates that the

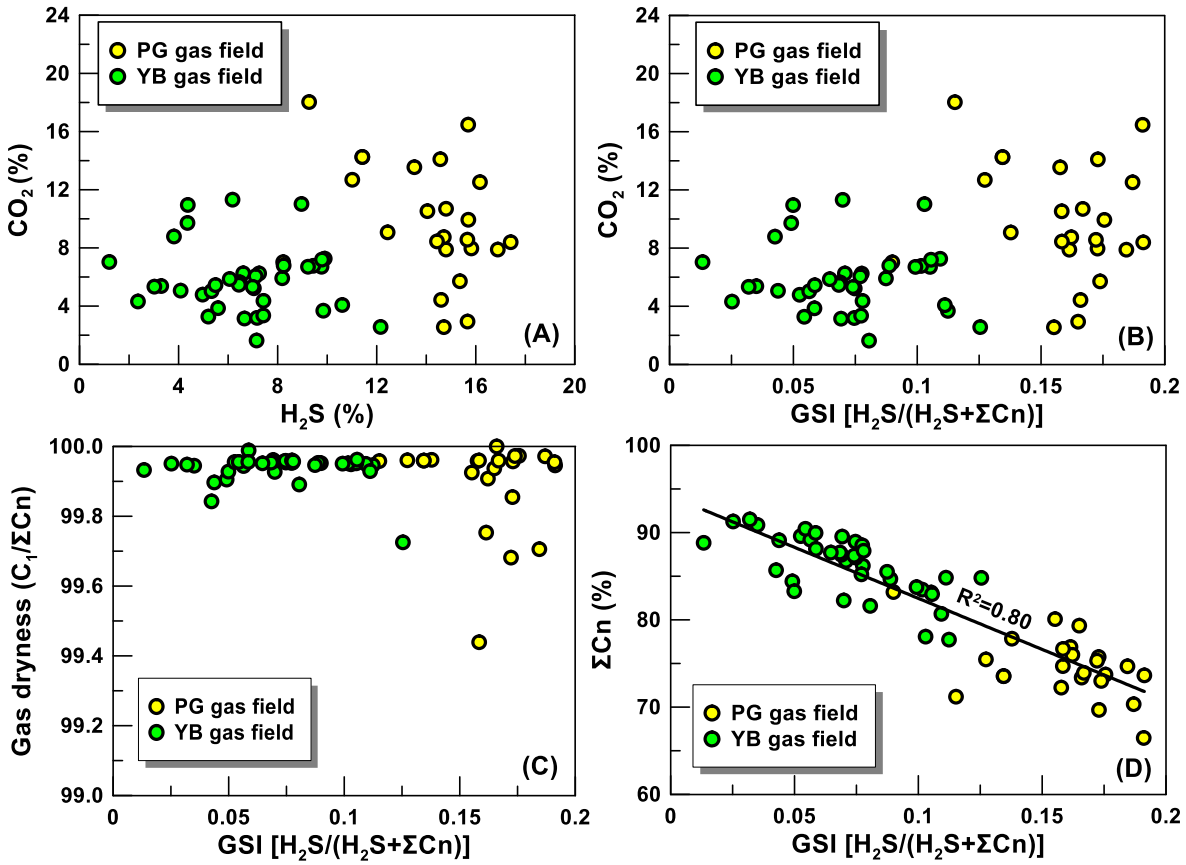

Fig. 4. Plots of (A) CO_2 vs H_2S, (B) CO_2 vs GSI, (C) Gas dryness vs GSI, and (D) $\sum$Cn vs GSI for the P_2c and T_1f gases from the Yuanba (YB) and Puguang (PG) gas fields. GSI = Gas souring index. The data for the PG gas field are from Hao et al. (2008) and Li et al. (2015), and the data for the YB gas field are from Li et al. (2015) and this study.

sulfate sources for the TSR in the PG and YB gas fields were most likely from the Early and Late T_1f, respectively. However, there is similar sulfur isotope fractionation between the T_1f anhydrite and solid bitumen in the PG and YB gas fields (6.7‰ and 5.5‰, respectively; Fig. 6), which seems to contradict the idea that no significant sulfur isotope fractionation occurred in the two gas fields due to the complete consumption of sulfates discussed above.

This is related to the fact that some of the organic sulfur derived from the kerogen in the source rock was mixed into the solid bitumen, resulting in the relatively low bulk $\delta^{34}S$ of the solid bitumen. The average $\delta^{34}S$ value of the unaltered solid bitumen from the P_2c and T_1f reservoirs in the northeastern Sichuan Basin is 7.7‰, and the S/C atomic ratio is 0.02 (Cai et al., 2017); while the average S/C atomic ratio of the TSR-altered solid bitumen from the PG and YB gas fields is 0.07 (Li et al., 2016). Thus, it can be determined that the ratio of the organic and inorganic sulfur in the solid bitumen in the PG and YB gas fields is about 2:5. As a result, the $\delta^{34}S$ values of the inorganic sulfur in the solid bitumen can be calculated based on the inorganic sulfur ratio and $\delta^{34}S$ values of the unaltered solid bitumen. The average $\delta^{34}S$ values of the inorganic sulfur in the solid bitumen from the PG and YB gas fields are 21.0‰ and 36.0‰, respectively, which are basically consistent with the $\delta^{34}S$ values of the Early and Late T_1f anhydrite (22.7‰ and 34.6‰; respectively). No significant sulfur isotope fractionation between the inorganic sulfur in the solid bitumen and the possible sulfates can support the sulfate-limited TSR discussed above.

The $\delta^{34}S$ value of the Late Permian-Early Triassic seawater worldwide gradually increased (Fig. 7) (Bernasconi et al., 2017), and the $\delta^{34}S$ values of the Early T_1f ($T_1f^{1\text{-}2}$) and Late T_1f ($T_1f^{3\text{-}4}$) seawater were 10.0–20.0‰ and 20.0–28.0‰, respectively (Fig. 7). The $\delta^{34}S$ values of the T_1f anhydrite in the Sichuan Basin were heavier than those of the co-eval seawater (Fig. 7), which may be related to the highly evaporative environment (Zhu et al., 2014). Based on the sulfur isotope fractionation and $\delta^{34}S$ value of the inorganic sulfur in the solid bitumen discussed above, the sulfate sources for the TSR in the PG and YB gas fields most likely originated from the Early T_1f ($T_1f^{1\text{-}2}$: $\delta^{34}S$ of 17.5–27.5‰) and Late T_1f (T_1f^{4}: $\delta^{34}S$ of 27.5–40.0‰) anhydrite and evaporative brine, respectively. In addition, the $\delta^{34}S$ values of the solid bitumen in the YB gas field are heavier than those of the Early T_1f anhydrite in the PG gas field, which also indicates that the sulfate for TSR in the YB gas field could not have been derived from the Early T_1f sulfate or brine.

Although there is partial overlap of the $\delta^{34}S$ values of the H_2S and solid bitumen, there is average sulfur isotope fractionation of 5.1‰ and 5.4‰ between the solid bitumen and H_2S in the PG and YB gas fields, respectively (Fig. 6). As is shown in Fig. 8, although the GSI values of the two gas fields are different, the differences in the $\delta^{34}S$ values of the solid bitumen and H_2S from the same well in the PG and YB gas fields are quite similar (averages of 6.2‰ and 6.0‰, respectively), which is similar to the average sulfur isotope fractionation between the solid bitumen and H_2S (5.1‰ and 5.4‰, Fig. 6). This indicates that there is indeed sulfur isotope fractionation between the solid bitumen and H_2S in the two gas fields; moreover, the sulfur isotope fractionation between the sulfates and H_2S is about 10.0‰, which is similar to reported the sulfur isotope fractionation vis TSR in the Sichuan Basin (Zhu et al., 2014).

The sulfur isotope fractionation between the solid bitumen and H_2S may be related to the fact that oil-dominated TSR (or limited wet gas and methane-dominated TSR) mainly occurred in the PG and YB gas fields, and the extent of the TSR was also similar in these two gas fields. During liquid hydrocarbon dominated-TSR, the inorganic sulfur from the sulfate

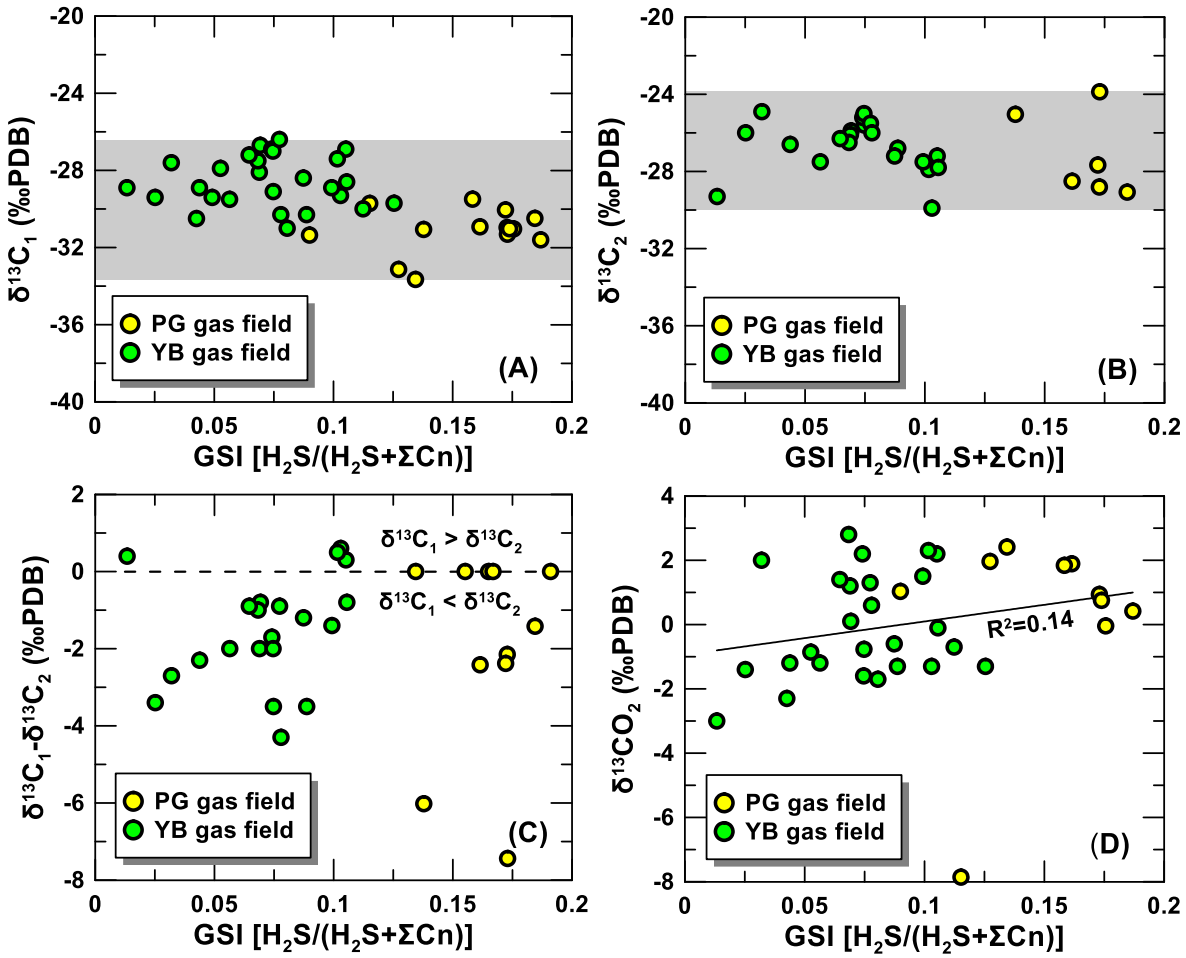

Fig. 5. Plots of (A) the carbon isotope ratios of the methane ($\delta^{13}C_1$) vs GSI, (B) the carbon isotope ratios of the ethane ($\delta^{13}C_2$) vs GSI, (C) the difference in the carbon isotope ratios of the methane and ethane ($\delta^{13}C_1$-$\delta^{13}C_2$) vs GSI, and (D) the carbon isotope ratios of the carbon dioxide (CO_2) vs GSI of the P_2c and T_1f gases from the Yuanba (YB) and Puguang (PG) gas fields. GSI = Gas souring index. The data for the PG gas field are from Hao et al. (2008) and Li et al. (2015), and the data for the YB gas field are from Li et al. (2015) and this study.

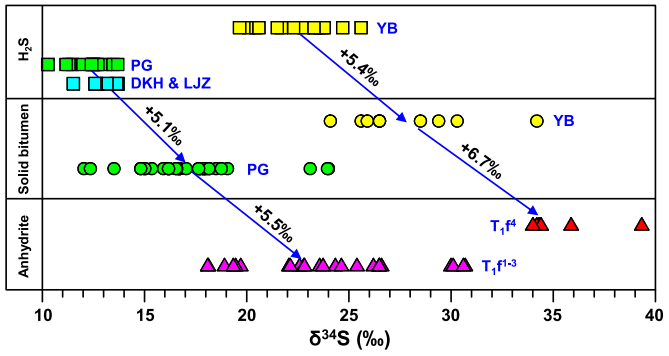

Fig. 6. Correlations between the sulfur isotope ratios ($\delta^{34}S$) of the H_2S, solid bitumen, and anhydrite samples from the NE Sichuan Basin. YB = Yuanba, PG = Puguang, LJZ = Luojiazhai, DKH = Dukouhe. $T_1f^{1\text{-}3}$ = the first to the third members of the Feixianguan Formation, T_1f^4 = the fourth member of the Feixianguan Formation. The data for H_2S samples from the PG, DKH and LJZ gas fields are from Wang et al. (2002), Zhu et al. (2005), Ma et al. (2008a, 2008b), and Zhu et al. (2008). The data for solid bitumen samples from the YB gas field are from Li et al. (2019), and the data for solid bitumen samples from the PG gas field are from Cai et al. (2010, 2017), Hao et al. (2015), and Li et al. (2019). The data for anhydrite samples are from Wang et al. (2002), Zhu et al. (2005), Zhu et al. (2008), Zhang (2009), and Li et al. (2019). The detailed data and sources are presented in Table 1S.

is mainly used to create solid bitumen and H_2S (R1). -, The TSR-associated ^{34}S-enriched H_2S back-reacts with the liquid oils, resulting in the generation of new secondary ^{34}S-enriched OSCs. With increasing burial depth and thermal stress, thermal cracking of these OSCs may produce relatively ^{34}S-enriched solid bitumen and ^{34}S-depleted H_2S later. This should be responsible for the occurrence of the ^{34}S-enriched solid bitumen relative to the H_2S in study area. However, a quantitative study of sulfur isotope fractionation between the solid bitumen and H_2S has not yet been reported. If wet gas and methane-dominated TSR (R2 and R3) progressed after the occurrence of liquid hydrocarbon dominated-TSR, the sulfur in the sulfate would be continually incorporated into the H_2S. This would result in a continuous increase in the $\delta^{34}S$ values of the H_2S, which would bring them closer to the $\delta^{34}S$ values of the sulfate and the $\delta^{34}S$ values of the H_2S would be even larger than those of the solid bitumen. In fact, the $\delta^{34}S$ values of the H_2S in the two gas fields are lower than those of the solid bitumen, and the differences between the $\delta^{34}S$ values of the solid bitumen and H_2S are quite similar (Fig. 6), indicating that liquid hydrocarbon dominated-TSR (or limited wet gas and methane-dominated TSR) mainly occurred in these two gas fields. Based on the sulfate sources for TSR determined in this study, the sulfur isotope fractionation between the sulfate and the H_2S produced by TSR in the PG and YB gas fields is 12.2‰ and 12.9‰, respectively. This is quite similar to the theoretical sulfur isotope fractionation at 160–170 °C (12.0‰–12.8‰; Kiyosu and Krouse, 1990), which is similar to the temperature at which crude oil begins to crack (~160 °C; Tian et al., 2008). This also suggests that liquid hydrocarbon dominated-TSR

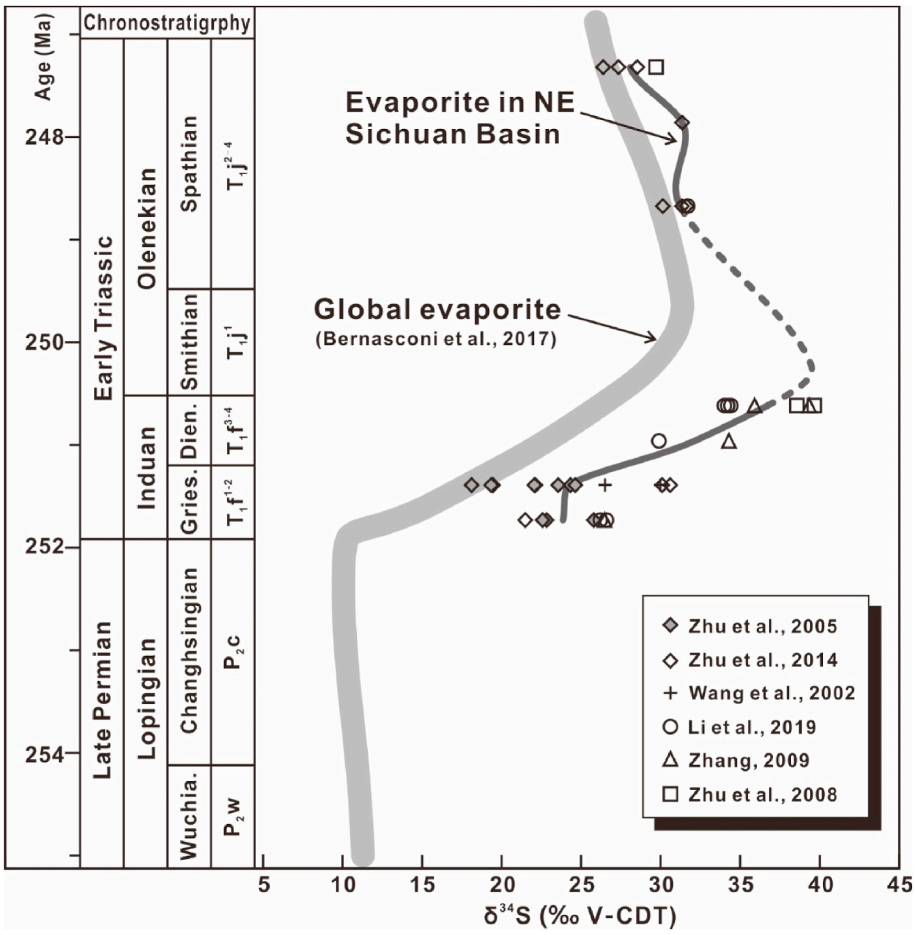

Fig. 7. Global sulfur isotope curve for the Late Permian to Early Triassic based on evaporites (from Bernasconi et al., 2017) and the sulfur isotope ratios of the Early Triassic evaporites in the NE Sichuan Basin.

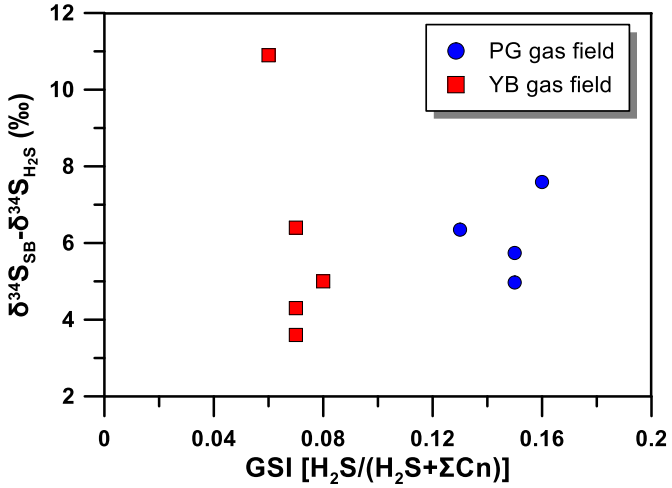

Fig. 8. Plots of the difference between the $\delta^{34}S$ values of the solid bitumen (SB) and H_2S vs GSI in the Yuanba (YB) and Puguang (PG) gas fields. All of the data are from the same single well. GSI = Gas souring index.

mainly occurred in the PG and YB gas fields.

In addition, the chemical and carbon isotope compositions of the hydrocarbon gases support the conclusion that liquid hydrocarbon dominated-TSR mainly occurred in these two gas fields. The roughly positive correlation between the concentrations of CO_2 and H_2S (Fig. 4A) and the negative correlation between the GSI and total hydrocarbon gases (Fig. 5C) suggest that TSR occurred in this area. As the GSI increases, the lighter ^{12}C in the hydrocarbons is preferentially oxidized during TSR (Hao et al., 2008). Theoretically, with the continuous conversion of liquid hydrocarbon-dominated TSR to wet gas and methane-dominated TSR, the $\delta^{13}C$ values of the residual ethane and methane may continue to increase. However, as the GSI increased, the $\delta^{13}C$ values of the methane and ethane did not significantly increase (Fig. 5A and B), suggesting that the contributions of the wet gas and methane-dominated TSR were limited in these two gas fields.

5.3. Enrichment of sulfates via dolomitization

All of the gas reservoirs with relatively high H_2S concentrations discovered thus far are dolostone gas reservoirs (Li et al., 2016), indicating that dolomitization is closely related to the enrichment of the sulfates required for TSR. Possible sources of the sulfates required for TSR include seawater, buried seawater, evaporative brine, and/or the dissolution of solid calcium sulfate (Machel et al., 1995). The P_2c-T_1f gas reservoirs and the gas-bearing structures in the limestone reservoirs in the Sichuan Basin do not contain H_2S, indicating that the sulfates required for the TSR in P_2c-T_1f were not derived from coeval seawater or buried seawater, and they were most likely from evaporative seawater (brine) and/or the dissolution of solid calcium sulfate.

What is the relationship between the enrichment of evaporative seawater and/or solid calcium sulfate and the dolomitization process? Based on the sulfate sources for TSR discussed in Section 5.2, the sulfates in the PG and YB gas fields were derived from the Early and Late T_1f evaporative platforms, respectively. For the eastern platform, the

evaporative brine from the Early T_1f evaporative platform could seep laterally into T_1f and P_2c on the platform's edge through the early selective dissolution pore system, which developed in the limestone at the edge of the platform (Fig. 9). For the western platform, the evaporative brine of T_1f^4 seeped vertically into the T_1f and P_2c on the platform's edge through syn-sedimentary fractures and an early selective dissolution pore system (Fig. 9). This seepage was mainly driven by the density difference between the evaporative brine and normal seawater (Li et al., 2021).

According to numerical simulations of the dolomitization process and geological observations, dolomitization caused by the reflux of brine can produce anhydrite precipitation (Jones and Xiao, 2005; Zhang, 2009; Jiang et al., 2013), and the amount of anhydrite precipitation is positively correlated with the scale of the dolomitization. The precipitated anhydrite and dissolved sulfate in the pore water may have been the main sulfate sources for TSR. There is a good positive correlation between the thickness of the T_1f-P_2c dolostone and the H_2S concentrations in these gas reservoirs in the Sichuan Basin ($R^2 = 0.75$; Fig. 10). In addition, the thermal evolution history of the gas reservoirs in the NE Sichuan Basin is similar (Fig. 3). The most likely reason for the difference in the concentration of H_2S in these gas reservoirs is the amount of sulfate. Large-scale dolomitization produces more anhydrite precipitation and evaporative brine (Jones and Xiao, 2005; Wang et al., 2021), resulting in sufficient SO_4^{2-} for TSR and causing more TSR and higher H_2S concentrations. Although most of the anhydrite cements produced in the dolostone reservoirs may have been consumed by TSR, remnants of anhydrite have been observed in the T_1f dolostone reservoirs in the PG gas field (Zhang, 2009; Jiang et al., 2014), which also

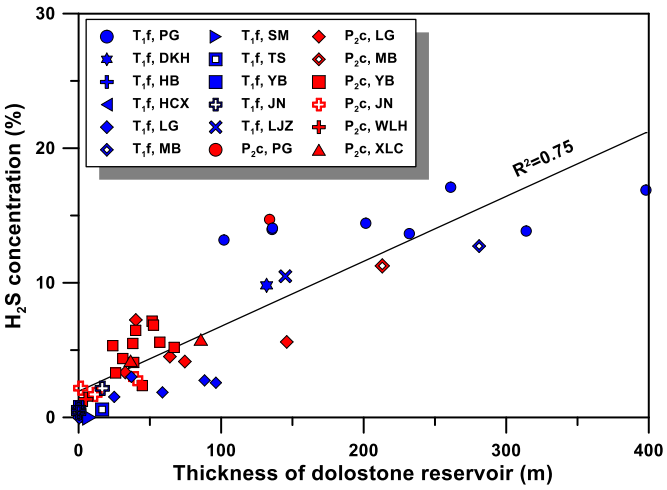

Fig. 10. Plot of H_2S concentration vs thickness of dolostone reservoir for typical gas fields and gas-bearing structures in the Sichuan Basin. T_1f = Feixianguan Formation, P_2c = Changxing Formation. DKH = Dukouhe, HCX = Huangcaoxia, HB = Heba, JN = Jiannan, LG = Longgang, LJZ = Luojiazhai, MB = Maoba, PG = Puguang, SM = Shuangmiao, TS = Tieshan, WLH = Wolonghe, XLC = Xinglongchang, YB = Yuanba.

indicates that the dissolution of these anhydrite cements provided part of the sulfate source for the TSR. In addition, the H_2S concentrations in the PG and YB gas fields (generally 5.0%–20.0%) are higher than the

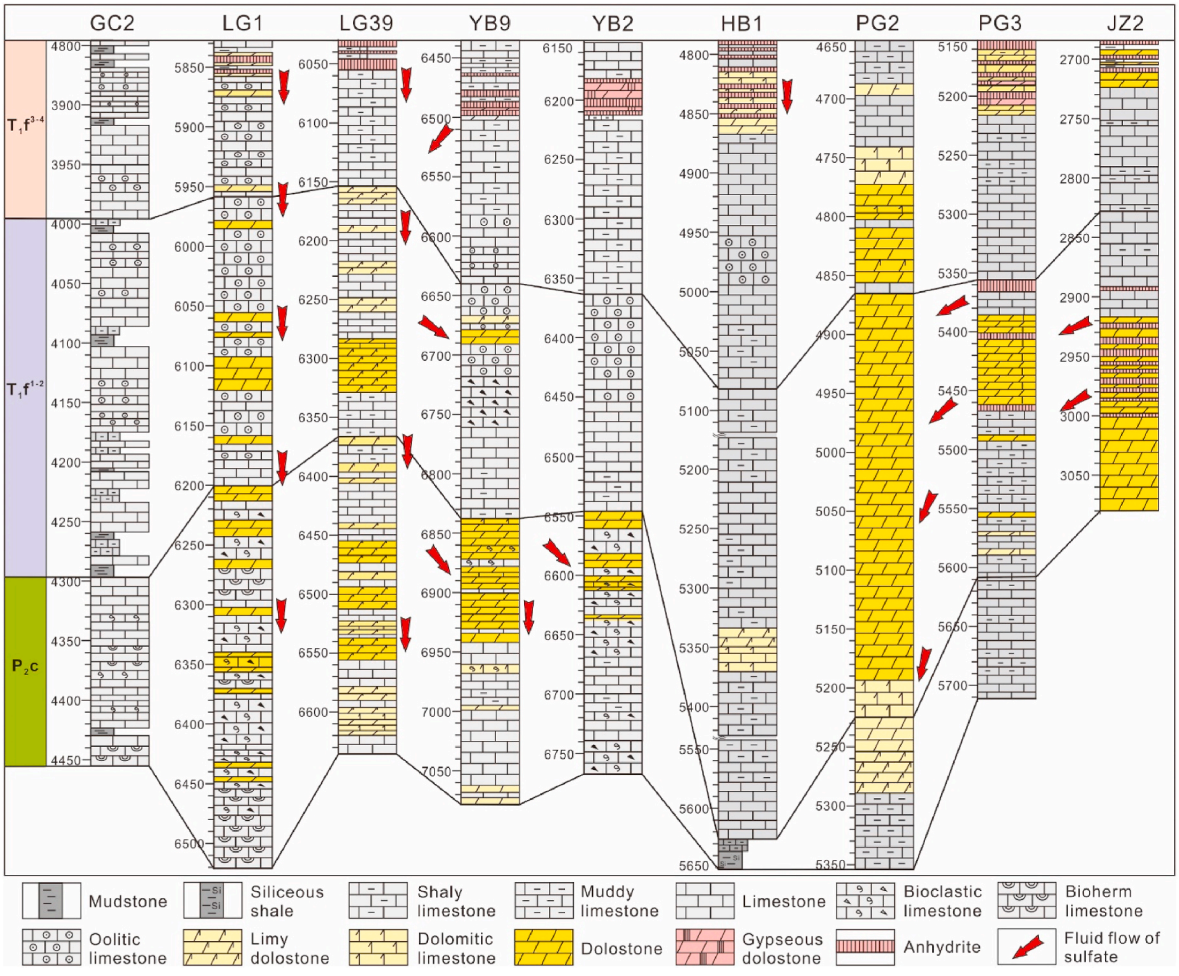

Fig. 9. Lithologic sections, possible sulfate sources, and flow model for the Puguang and Yuanba gas fields in the NE Sichuan Basin.

H_2S concentrations in the JN gas field (<5.0%). However, the SO_4^{2-} concentrations of the T_1f-P_2c formation water in the PG and YB gas fields (0–1.47 g/L) are lower than those of the T_1f formation water in the JN gas field (1.48–4.06 g/L) (Li et al., 2016). This indicates that the SO_4^{2-} in the formation water of the PG and YB gas fields was consumed by the TSR reaction.

Except for the SO_4^{2-} and anhydrite precipitation produced by dolomitization, the higher H_2S concentrations of the dolostone reservoirs may also be related to the Mg^{2+} enrichment during dolomitizationbecause the magnesium sulfate contact ion-pairs ($[MgSO_4]_{CIP}$) can be more reactive than free sulfate ions (SO_4^{2-}) and can be more favorable for TSR (Pan et al., 2006; Ma et al., 2008a; Lu et al., 2011; Liu et al., 2020). Unlike other H_2S enriched gas reservoirs associated with layered anhydrite, which supply sufficient sulfate for TSR via direct dissolution of these anhydrite layers (Videtich, 1994; Worden and Smalley, 1996; Heydari, 1997), the sulfate source in the Sichuan Basin may be insufficient. This may be the main reason for the relatively low H_2S concentrations in this area.

The sulfate sources for TSR and its enrichment during the dolomitization process summarized above are also supported by the petrology and geochemical data for the T_1f-P_2c dolostone. First, numerous selective freshwater dissolution pores occur in the T_1f-P_2c dolostone in both the eastern and western platform edges (Ma et al., 2007; Zhang, 2009; Li et al., 2021), suggesting that the dolomitization occurred at quite shallow burial depths or under near surface conditions; otherwise, the early dissolution pores would be destroyed by carbonate cements during the late burial stage. The early selective dissolution pore system ensured the continual lateral seepage of the evaporative brine from the Early T_1f evaporative platform, causing large-scale dolomitization, enrichment of SO_4^{2-} bearing brine, and gypsum deposition. In addition, the Sr isotope ratios ($^{87}Sr/^{86}Sr$) of the T_1f and P_2c dolostones in the eastern platform are similar and are very close to the Sr isotope ratios of the Early T_1f seawater (Zheng et al., 2009; Li et al., 2014, 2021). According to the Sr isotope evolution, the Sr isotope ratios increased continuously from the Late Permian to Early Triassic (McArthur et al., 2012). Thus, the dolomitizing fluids of the P_2c dolostone originated from the Early Triassic brine through lateral seepage. Similarly, the Sr isotope ratios of the P_2c dolostone in the western platform are significantly heavier than those of the coeval P_2c seawater, but they are close to those of the Late T_1f seawater, suggesting that the dolomitizing fluids originated from the ^{87}Sr enriched Late T_1f seawater (Li et al., 2021).

Based on the correlations between the sulfur isotope ratios of the solid sulfate, solid bitumen, and H_2S, the sulfate source for TSR was determined, and it is quite consistent with the sources of the dolomitizing fluid. This suggests that the sulfates for TSR were enriched during the dolomitization process, which is supported by the positive relationship between the thickness of the dolostone and the H_2S concentration. This finding provides a basic rule for predicting the distribution of H_2S within an evaporative platform (the original sulfate source) and during dolomitization.

5.4. *Prediction of the H_2S distribution in P_2c and T_1f in the Sichuan Basin*

TSR is a reaction between hydrocarbons and sulfate (Orr, 1974; Machel et al., 1995), therefore, the H_2S produced by TSR is controlled by both the hydrocarbons and sulfate. According to the above discussion, the TSR in the T_1f and P_2c reservoirs in the Sichuan Basin most likely mainly occurred during the liquid hydrocarbon dominated-TSR stage. Therefore, the accumulation of paleo-oil and the presence of sufficient sulfate are the keys to determining the distribution of H_2S. The sulfates for the TSR were mainly derived from the Early and Late T_1f evaporative platforms. As a result, the distribution of the T_1f evaporative platform limits the lateral distribution of the H_2S. According to the abundant drilling data, the Early T_1f ($T_1f^{1\text{-}2}$) evaporative platform containing anhydrite layers was mainly developed on the eastern platform (Fig. 11A), while the Late T_1f (T_1f^4) evaporative platform containing anhydrite layers was mainly distributed in a large area in the northeastern Sichuan Basin (Fig. 11B).

The accumulation of paleo-oil in the T_1f-P_2c dolostone reservoir in the Sichuan Basin mainly occurred in the Late Triassic to Early Jurassic (Guo et al., 2014). During this period, the structural setting of the northeastern Sichuan was relatively stable. Thus, the accumulation of paleo-oil mainly occurred in the platform edges, which were favorable environments for the formation of dolostone reservoirs and oil accumulations due to the adjacent hydrocarbon generation centers in the Permian source rock (Guo et al., 2014).

The sulfate source depends on the distribution of the T_1f evaporative platform. The Early T_1f evaporative platform was mainly distributed in the eastern area, while the Late T_1f evaporative platform was distributed in a large area in the northeastern Sichuan Basin (Du et al., 2010). The T_1f-P_2c gas reservoirs or fields with high H_2S concentrations, such as the MB, PG, QLB, DKH, LJZ, WBT, GFC, TSP, and other gas reservoirs and

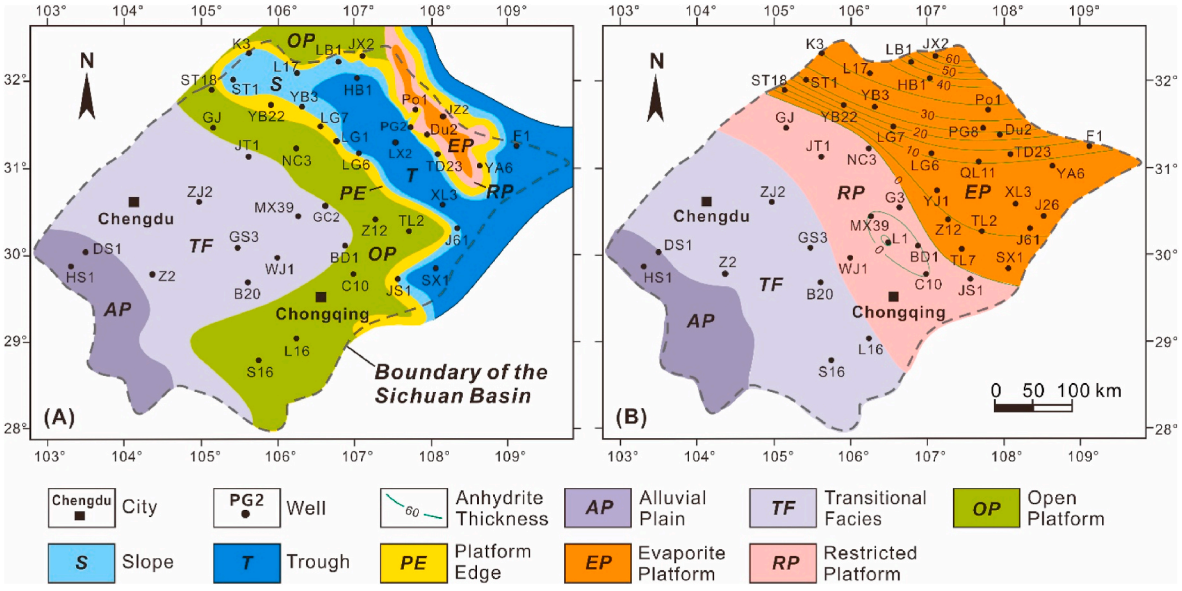

Fig. 11. Sedimentary facies of the (A) second and (B) fourth members of the Feixianguan Formation (T_1f) in the Sichuan Basin. The thickness of the anhydrite in the fourth member of T_1f is also shown in B.

fields discovered in the eastern platform are all located on the edge of the eastern platform, and they are adjacent to the Early T_1f evaporative platform. However, several gas fields and gas-bearing structures are located beyond the edge of the eastern platform, such as the HB, DYZ, QXC, and SGP, and they do not contain H_2S due to a lack of dolostone reservoirs and sufficient sulfates (Fig. 12A).

The sulfates for TSR were mainly derived from the T_1f^4 evaporative platform on the western platform. The H_2S-bearing gas fields discovered thus far are also located within the distribution range of the T_1f^4 evaporative platform (Fig. 12B), which supports the conclusion that the T_1f^4 evaporative platform provided the sulfate source for the TSR. The H_2S concentrations of the P_2c-T_1f natural gases in the BD, XS, TLX, HCX, and SL gas reservoirs and in well LS1, which are not located in the distribution range of the T_1f^4 anhydrite, are lower than 0.1% or close to zero (Fig. 12B). Therefore, we can use the area of overlap of the T_1f^4 anhydrite and the western platform (including platform edges and open platform) to predict the distribution range of the P_2c-T_1f H_2S in the western platform (Fig. 12B). All of the H_2S-bearing gas reservoirs should be within this overlap area, and the H_2S concentrations exhibit relatively large heterogeneity. For the H_2S-rich gas reservoirs located in the

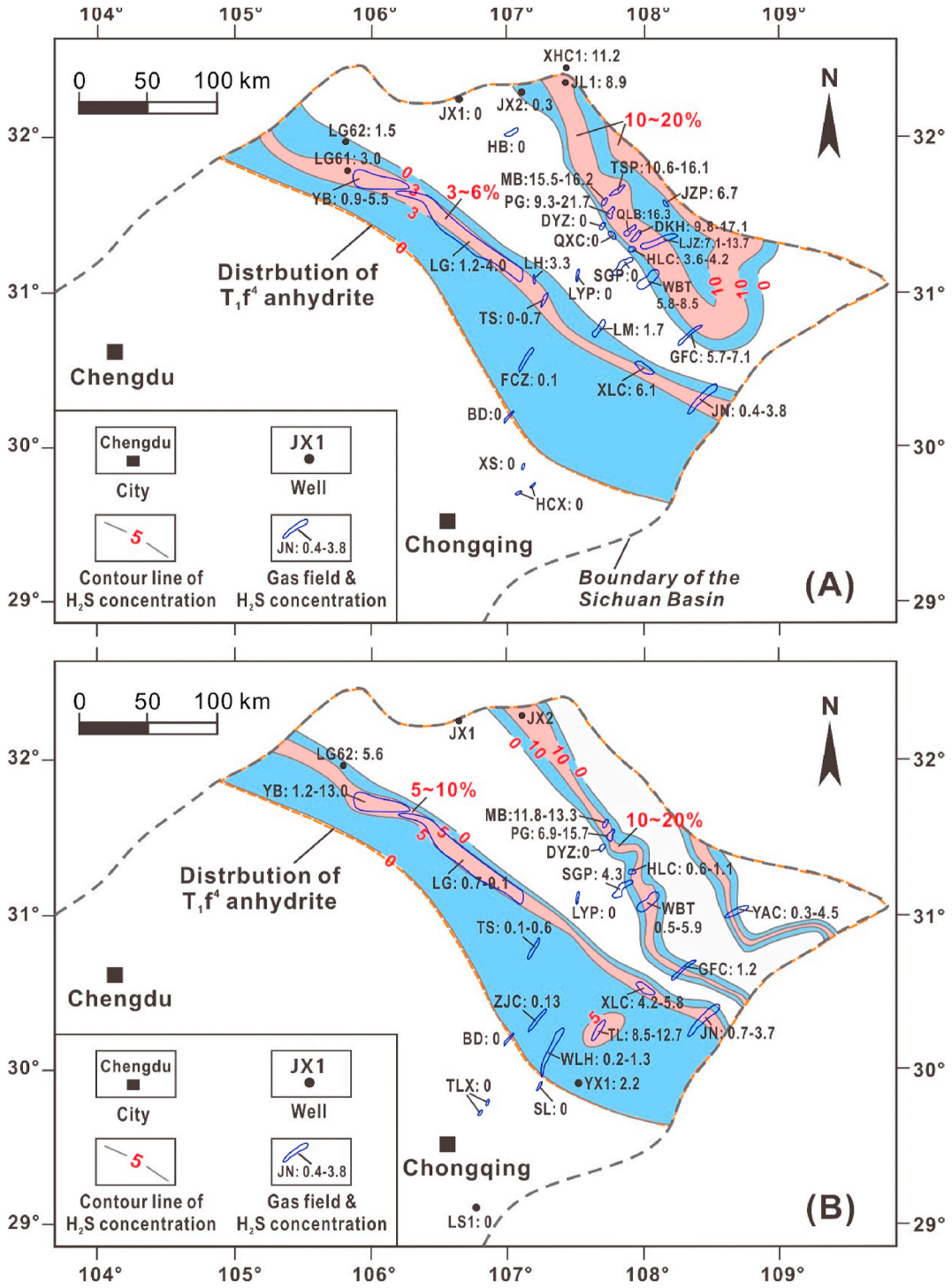

Fig. 12. H_2S concentrations in typical gas fields, gas-bearing structures, and wells in the (A) Feixianguan Formation and (B) Changxing Formation in the Sichuan Basin. The detailed data and sources are presented in Tables 2S.

platform's edge, such as the YB, LG, XCL, and other gas reservoirs, the sulfate enrichment was developed due to relatively large-scale dolomitization, and the paleo-oil accumulations are favorable because they are adjacent to the hydrocarbon-generating centers. As a result, the extents of the TSR in these reservoirs were higher, producing higher H_2S concentrations (5%–10%, Fig. 12B). For the gas reservoirs located in the open platform on the southwestern side of the platform's edge, the H_2S concentrations are relatively low (<5.0%) due to insufficient sulfates and/or lack of paleo-oil accumulations. For the gas reservoirs located in the southwestern part of the open platform and beyond the pinch-out line of the T_1f^4 anhydrite, the possibility of encountering H_2S is extremely low because there was no sulfate source in this area (Fig. 12B).

In addition, the present H_2S discovered in the gas reservoirs is the result of their geological history. If the preservation conditions of the gas reservoirs were destroyed after the occurrence of TSR, the H_2S may accumulate in other reservoirs that are laterally or vertically adjacent to the original H_2S-bearing gas reservoirs. Therefore, it is theoretically possible that H_2S may occur in the non-dolomitized intervals. Consequently, the preservation conditions of the H_2S-bearing gas reservoirs should be carefully evaluated during the prediction of the H_2S distribution.

6. Conclusions

The main conclusions of this study are as follows.

(1) The relatively high H_2S concentrations (mainly between 5.0% and 20.0%) and $\delta^{34}S$ values of the solid bitumen (mainly between 12.0% and 31.0%) and H_2S (mainly between 10.0% and 26.0%), which are significantly heavier than those of the kerogen in the Permian source rock indicate that the H_2S in the YB and PG gas fields has a TSR origin.
(2) The $\delta^{34}S$ values of the solid bitumen and H_2S in the PG gas field in the eastern platform are lower than the $\delta^{34}S$ values of the solid bitumen and H_2S in the YB gas field in the western platform. The sulfates for the TSR originated from the Early and Late T_1f evaporative platforms, respectively.
(3) There is no significant increase in the $\delta^{13}C$ values of the ethane and methane as the GSI increases, and the $\delta^{34}S$ values of the solid bitumen are heavier than those of the H_2S in the YB and PG gas fields, indicating that the TSR mainly occurred in the liquid hydrocarbon dominated-TSR stage.
(4) The positive correlation between the H_2S concentrations and the thickness of the dolostone reservoirs (or the scale of dolomitization) suggests that the sulfate (SO_4^{2-} bearing brine and gypsum deposits) for the TSR was most likely enriched during the dolomitization.
(5) The distributions of the T_1f anhydrite and the paleo-oil accumulations affect the distribution of the H_2S. For the eastern platform, the H_2S-bearing gas reservoirs in P_2c-T_1f are mainly located in the platform's edge and surround the Early T_1f evaporative platform; while for the western platform, the H_2S-bearing gas reservoirs are mainly located in the area surrounded by the platform's edge and the pinch-out line of the Late T_1f anhydrite.

Credit author statement

Pingping Li, Conceptualization, Investigation, Methodology, Writing- Original Draft. Bisong Li, Jinbao Duan, Resources. Yizhen Zhao, Experiment. Huayao Zou, Supervision, Funding acquisition. Fang Hao, Project administration.

Declaration of competing interest

The authors declare that they have no known competing financial interests or personal relationships that could have appeared to influence the work reported in this paper.

Data availability

Data will be made available on request.

Acknowledgments

This study was supported by the NSFC Basic Research Program on Deep Petroleum Resource Accumulation and Key Engineering Technologies (U19B6003) and the Strategic Priority Research Program of the Chinese Academy of Sciences (XDA14010306). We acknowledge the support provided by Zhongping Li and Lantian Xing from the Northwest Institute of Eco-Environment and Resources (Chinese Academy of Sciences) in the chemical and isotopic composition analyses of the natural gas samples. We thank Kenneth E. Peters and three other anonymous reviewers for their thorough and critical reviews which greatly improved the quality of this manuscript.

Appendix A. Supplementary data

Supplementary data related to this article can be found at https://doi.org/10.1016/j.marpetgeo.2022.105892.

References

Amrani, A., Lewan, M.D., Aizenshtat, Z., 2005. Stable sulfur isotope partitioning during simulated petroleum formation as determined by hydrous pyrolysis of Ghareb Limestone, Israel. Geochem. Cosmochim. Acta 69, 5317–5331.
Bahadori, A., 2014. Chapter 11-sulfur recovery. In: Bahadori, A. (Ed.), Natural Gas Processing. Waltham, Gulf Professional Publishing, pp. 519–546.
Bernasconi, S.M., Meier, I., Wohlwend, S., Brack, P., Hochuli, P.A., Bläsi, H., Wortmann, U.G., Ramseyer, K., 2017. An evaporite-based high-resolution sulfur isotope record of Late Permian and Triassic seawater sulfate. Geochem. Cosmochim. Acta 204, 331–349. https://doi.org/10.1016/j.gca.2017.01.047.
Bildstein, O., Worden, R.H., Brosse, E., 2001. Assessment of anhydrite dissolution as the rate-limiting step during thermochemical sulfate reduction. Chem. Geol. 176, 173–189. https://doi.org/10.1016/S0009-2541(00)00398-3.
Cai, C.F., Li, K.K., Zhu, Y.M., Xiang, L., Jiang, L., Tenger, Cai, X.Y., Cai, L.L., 2010. TSR origin of sulfur in Permian and Triassic reservoir bitumen, East Sichuan Basin, China. Org. Geochem. 41, 871–878. https://doi.org/10.1016/j.orggeochem.2010.03.009.
Cai, C.F., Xiang, L., Yuan, Y.Y., Xu, C.L., He, W.X., Tang, Y.J., Borjigin, T., 2017. Sulfur and carbon isotopic compositions of the Permian to Triassic TSR and non-TSR altered solid bitumen and its parent source rock in NE Sichuan Basin. Org. Geochem. 105, 1–12. https://doi.org/10.1016/j.orggeochem.2016.12.004.
Du, J.H., Xu, C.C., Wang, Z.C., Shen, P., He, H.Q., Yang, Y., Li, Z.R., Luo, Z., Zhou, J.G., 2010. Natural Gas Exploration of Permian-Triassic Reef & Oolite in Sichuan Basin. Petroleum Industry Press, Beijing, p. 160.
Guo, X.S., Hu, D.F., Li, Y.P., Duan, J.B., Ji, C.H., Duan, H., 2018. Discovery and theoretical and technical innovations of Yuanba gas filed in Sichuan Basin, SW China. Petrol. Explor. Dev. 45, 15–28.
Guo, X.S., Huang, R.C., Fu, X.Y., Duan, J.B., 2014. Gas accumulation and exploration direction of the Permian and Triassic reservoirs of reef-ban facies in Sichuan Basin. Oil Gas Geol. 35, 295–302 (in Chinese with English abstract).
Hao, F., Guo, T.L., Zhu, Y.M., Cai, X.Y., Zou, H.Y., Li, P.P., 2008. Evidence for multiple stages of oil cracking and thermochemical sulfate reduction in the Puguang gas field, Sichuan Basin, China. AAPG (Am. Assoc. Pet. Geol.) Bull. 92, 611–637. https://doi.org/10.1306/01210807090.
Hao, F., Zhang, X.F., Wang, C.W., Li, P.P., Guo, T.L., Zou, H.Y., Zhu, Y.M., Liu, J.Z., Cai, Z.X., 2015. The fate of CO_2 derived from thermochemical sulfate reduction (TSR) and effect of TSR on carbonate porosity and permeability, Sichuan Basin, China. Earth Sci. Rev. 141, 154–177. https://doi.org/10.1016/j.earscirev.2014.12.001.
Harrison, A.G., Thode, H.G., 1957. The kinetic isotope effect in the chemical reduction of sulphate. Trans. Faraday Soc. 53, 1648–1651.
Heydari, E., Moore, C.H., 1989. Burial diagenesis and thermochemical sulfate reduction. Smackover Formation, south eastern Mississippi salt basin. Geology 17, 1080–1084.
Heydari, E., 1997. The role of burial diagenesis in hydrocarbon destruction and H_2S accumulation, Upper Jurassic smackover formation, Black Creek field, Mississippi. AAPG (Am. Assoc. Pet. Geol.) Bull. 81, 26–45. https://doi.org/10.1306/522B427B-1727-11D7-8645000102C1865D.
Huang, H.Y., He, D.F., Li, Y.Q., Wang, B., 2017. The prototype and its evolution of the Sichuan sedimentary basin and adjacent areas during Liangshan and Qixia stages in Permian. Acta Petrol. Sin. 33, 1317–1337 (in Chinese with English abstract).
Idiz, E.F., Tannenbaum, E., Kaplan, I.R., 1990. Pyrolysis of high-sulfur Monterey kerogens - stable isotopes of sulfur, carbon, and hydrogen. In: Orr, W.L., White, C.M. (Eds.), Geochem. Sulf. Fossil Fuels ACS Symp. Ser. 429, 575–591.

Jenden, P.D., Titley, P.A., Worden, R.H., 2015. Enrichment of nitrogen and ^{13}C of methane in natural gases from the Khuff Formation, Saudi Arabia, caused by thermochemical sulfate reduction. Org. Geochem. 82, 54–68. https://doi.org/10.1016/j.orggeochem.2015.02.008.

Jiang, L., Cai, C.F., Worden, R.H., Li, K.K., Xiang, L., 2013. Reflux dolomitization of the Upper Permian Changxing Formation and the lower Triassic Feixianguan formation, NE Sichuan Basin, China. Geofluids 13, 232–245. https://doi.org/10.1111/gfl.12034.

Jiang, L., Worden, R.H., Cai, C.F., 2014. Thermochemical sulfate reduction and fluid evolution of the Lower Triassic Feixianguan Formation sour gas reservoirs, northeast Sichuan Basin, China. AAPG (Am. Assoc. Pet. Geol.) Bull. 98, 947–973. https://doi.org/10.1306/10171312220.

Jones, G.D., Xiao, Y., 2005. Dolomitization, anhydrite cementation, and porosity evolution in a reflux system: insights from reactive transport models. AAPG (Am. Assoc. Pet. Geol.) Bull. 89, 577–601. https://doi.org/10.1306/12010404078.

Kelemen, S.R., Walters, C.C., Kwiatek, P.J., Afeworki, M., Sansone, M., Freund, H., Pottorf, R.J., Machel, H.G., Zhang, T.W., Ellis, G.S., Tang, Y.C., Peters, K.E., 2008. Distinguishing solid bitumens formed by thermochemical sulfate reduction and thermal chemical alteration. Org. Geochem. 39, 1137–1143. https://doi.org/10.1016/j.orggeochem.2008.04.007.

King, H.E., Walters, C.C., Horn, W.C., Zimmer, M., Heines, M.M., Lamberti, W.A., Kliewer, C., Pottorf, R.J., Macleod, G., 2014. Sulfur isotope analysis of bitumen and pyrite associated with thermal sulfate reduction in reservoir carbonates at the Big Piney–La Barge production complex. Geochem. Cosmochim. Acta 134, 210–220. https://doi.org/10.1016/j.gca.2013.11.005.

Kiyosu, Y., Krouse, H.R., 1990. The role of organic acid in the abiogenic reduction of sulfate and the sulfur isotope effect. Geochem. J. 24, 21–27. https://doi.org/10.2343/geochemj.24.21.

Li, J., Xie, Z.Y., Dai, J.X., Zhang, S.C., Zhu, G.Y., Liu, Z.L., 2005. Geochemistry and origin of sour gas accumulations in the northeastern Sichuan Basin, SW China. Org. Geochem. 36, 1703–1716. https://doi.org/10.1016/j.orggeochem.2005.08.006.

Li, K.K., Cai, C.F., Hou, D.J., He, X.Y., Jiang, L., Jia, L.Q., Cai, L., 2014. Origin of high H_2S concentrations in the Upper Permian Changxing reservoirs of the northeast Sichuan Basin, China. Mar. Petrol. Geol. 57, 233–243. https://doi.org/10.1016/j.marpetgeo.2014.05.011.

Li, P.P., Hao, F., Guo, X.S., Zou, H.Y., Yu, X.Y., Wang, G.W., 2015. Processes involved in the origin and accumulation of hydrocarbon gases in the Yuanba gas field, Sichuan Basin, southwest China. Mar. Petrol. Geol. 59, 150–165. https://doi.org/10.1016/j.marpetgeo.2014.08.003.

Li, P.P., Hao, F., Guo, X.S., Zou, H.Y., Zhu, Y.M., Yu, X.Y., Wang, G.W., 2016. Origin and distribution of hydrogen sulfide in the Yuanba gas field, Sichuan Basin, Southwest China. Mar. Petrol. Geol. 75, 220–239. https://doi.org/10.1016/j.marpetgeo.2016.04.021.

Li, P.P., Zou, H.Y., Hao, F., Yu, X.Y., 2019. Sulfate sources of thermal sulfate reduction (TSR) in the Permian Changxing and Triassic Feixianguan formations, northeastern Sichuan Basin, China. Geofluids 5898901, 13. https://doi.org/10.1155/2019/5898901, 2019.

Li, P.P., Zou, H.Y., Yu, X.Y., Hao, F., Wang, G.W., 2021. Source of dolomitizing fluids and dolomitization model of the Upper Permian Changxing and lower Triassic Feixianguan formations, NE Sichuan Basin, China. Mar. Petrol. Geol. 125 (104834), 15. https://doi.org/10.1016/j.marpetgeo.2020.104834.

Liu, S.G., Yang, Y., Deng, B., Zhong, Y., Wen, L., Sun, W., Li, Z.W., Jansa, L., Li, J.X., Song, J.M., Zhang, X.H., Peng, H.L., 2021. Tectonic evolution of the Sichuan Basin, southwest China. Earth Sci. Rev. 213 (103470), 18. https://doi.org/10.1016/j.earscirev.2020.103470.

Liu, Q.Y., Peng, W.L., Meng, Q.Q., Zhu, D.Y., Jin, J.Z., Wu, X.Q., 2020. Fractionation of carbon and hydrogen isotopes of TSR-altered gas products under closed system pyrolysis. Scientific Reports 10, 12921. https://doi.org/10.1038/s41598-020-69580-0.

Liu, Q.Y., Worden, R.H., Jin, Z.J., Liu, W.H., Li, J., Gao, B., Zhang, D.W., Hu, A.P., Yang, C., 2013. TSR versus non-TSR processes and their impact on gas geochemistry and carbon stable isotopes in Carboniferous, Permian and Lower Triassic marine carbonate gas reservoirs in the Eastern Sichuan Basin, China. Geochem. Cosmochim. Acta 100, 96–115. https://doi.org/10.1016/j.gca.2012.09.039.

Liu, Q.Y., Jin, Z.J., Wu, X.Q., Liu, W.H., Gao, B., Zhang, D.W., Li, J., Hu, A.P., 2014a. Origin and carbon isotope fractionation of CO_2 in marine sour gas reservoirs in the Eastern Sichuan Basin. Org. Geochem. 74, 22–32. https://doi.org/10.1016/j.orggeochem.2014.01.012.

Liu, Q.Y., Jin, Z.J., Wu, X.Q., Lin, J.H., Gao, B., Zhang, D.W., Xu, M.E., 2014b. Origin and filling model of natural gas in Jiannan gas field, Sichuan Basin, China. Energy Explor. Exploit. 32, 569–590.

Liu, Q.Y., Worden, R.H., Jin, Z.J., Liu, W.H., Li, J., Gao, B., Zhang, D.W., Hu, A.P., Yang, C., 2014c. Thermochemical sulphate reduction (TSR) versus maturation and their effects on hydrogen stable isotopes of very dry alkane gases. Geochem. Cosmochim. Acta 137, 208–220.

Liu, Q.Y., Wu, X.Q., Wang, X.F., Jin, Z.J., Zhu, D.Y., Meng, Q.Q., Huang, S.P., Liu, J.Y., Fu, Q., 2019. Carbon and hydrogen isotopes of methane, ethane, and propane: a review of genetic identification of natural gas. Earth Sci. Rev. 190, 247–272.

Lu, H., Greenwood, P., Chen, T.S., Liu, J.Z., Peng, P.A., 2011. The role of metal sulfates in thermochemical sulfate reduction (TSR) of hydrocarbons: insight from the yields and stable carbon isotopes of gas products. Org. Geochem. 42, 700–706. https://doi.org/10.1016/j.orggeochem.2011.03.011.

Ma, Q.S., Ellis, G.S., Amrani, A., Zhang, T.W., Tang, Y.C., 2008a. Theoretical study on the reactivity of sulfate species with hydrocarbons. Geochem. Cosmochim. Acta 72, 4565–4576. https://doi.org/10.1016/j.gca.2008.05.061.

Ma, Y.S., Guo, X.S., Guo, T.L., Huang, R., Cai, X.Y., Li, G.X., 2007. The Puguang gas field-New giant discovery in the mature Sichuan Basin, SW China. AAPG (Am. Assoc. Pet. Geol.) Bull. 91, 627–643.

Ma, Y.S., Zhang, S.C., Guo, T.L., Zhu, G.Y., Cai, X.Y., Li, M.W., 2008b. Petroleum geology of the Puguang sour gas field in the Sichuan Basin, SW China. Mar. Petrol. Geol. 25, 357–370. https://doi.org/10.1016/j.marpetgeo.2008.01.010.

Machel, H.G., 1987. Some aspects of diagenetic sulphate-hydrocarbon redox-reactions. In: Marshall, J.D. (Ed.), Diagenesis of Sedimentary Sequences. Geological Society Special Publication, Boston, pp. 15–28. Blackwell Scientific Publications.

Machel, H.G., 2001. Bacterial and thermochemical sulfate reduction in diagenetic settings–old and new insights. Sediment. Geol. 140, 143–175. https://doi.org/10.1016/S0037-0738(00)00176-7.

Machel, H.G., Krouse, H.R., Sassen, R., 1995. Products and distinguishing criteria of bacterial and thermochemical sulfate reduction. Appl. Geochem. 10, 373–389. https://doi.org/10.1016/0883-2927(95)00008-8.

McArthur, J.M., Howarth, R.J., Shields, G.A., 2012. Strontium isotope stratigraphy. In: Gradstein, F.M., Ogg, J.G., Schmitz, M., Ogg, G.M. (Eds.), The Geologic Time Scale 2012, vol. 2. Elsevier, Amsterdam, pp. 127–144.

Meshoulam, A., Ellis, G.S., Ahmad, W.S., Deev, A., Sessions, A.L., Tang, Y.C., Adkins, J.F., Liu, J.Z., Gilhooly, W.P., Aizenshtat, Z., Amrani, A., 2016. Study of thermochemical sulfate reduction mechanism using compound specific sulfur isotope analysis. Geochem. Cosmochim. Acta 188, 73–92.

Orr, W.L., 1974. Changes in sulfur content and isotopic ratios of sulfur during petroleum maturation–study of Big Horn Basin Paleozoic oils. AAPG (Am. Assoc. Pet. Geol.) Bull. 58, 2295–2318. https://doi.org/10.1306/83D91B9B-16C7-11D7-8645000102C1865D.

Orr, W.L., 1977. Geologic and geochemical controls on the distribution of hydrogen sulfide in natural gas. In: Campos, R., Goni, J. (Eds.), Advances in Organic Geochemistry. Enadisma, Madrid, pp. 571–597.

Orr, W.L., 1986. Kerogen asphaltene sulfur relationships in sulfur-rich Monterey oils. Org. Geochem. 10, 499–516.

Pan, C.C., Yu, L.P., Liu, J.Z., Fu, J.M., 2006. Chemical and carbon isotopic fractionations of gaseous hydrocarbons during abiogenic oxidation. Earth Planet Sci. Lett. 246, 70–89.

Rosenberg, Y.O., Meshoulam, A., Said-Ahmad, W., Shawar, L., Dror, G., Reznik, I.J., Feinstein, S., Amrani, A., 2017. Study of thermal maturation processes of sulfur-rich source rock using compound specific sulfur isotope analysis. Org. Geochem. 112, 59–74.

Shellnutt, J.G., 2014. The Emeishan large igneous province: a synthesis. Geosci. Front. 5, 369–394. https://doi.org/10.1016/j.gsf.2013.07.003.

Shu, Z.G., 2014. The discovery of the Jiannan shelf in the southeastern part of the Kaijiang-Liangping shelf. Sediment. Geol. Tethyan Geol. 34, 1–8 (in Chinese with English abstract).

Sweeney, J.J., Burnham, A.K., 1990. Evaluation of a simple model of vitrinite reflectance based on chemical kinetics. AAPG (Am. Assoc. Pet. Geol.) Bull. 74, 1559–1570.

Tian, H., Xiao, X.M., Wilkins, R.W.T., Tang, Y.C., 2008. New insights into the volume and pressure changes during the thermal cracking of oil to gas in reservoirs: implications for the in-situ accumulation of gas cracked from oils. AAPG (Am. Assoc. Pet. Geol.) Bull. 92, 181–200. https://doi.org/10.1306/09210706140.

Videtich, P.E., 1994. Dolomitization and H_2S generation in the Permian Khuff formation, Offshore Dubai, U.A.E. Carbonat. Evap. 9, 42–57. https://doi.org/10.1007/bf03175185.

Wang, X.Z., Li, B., Wen, L., Xu, L., Xie, S.Y., Du, Y., Feng, M.Y., Yang, X.F., Wang, Y.P., Pei, S.Q., 2021. Characteristics of "Guangyuan-Wangcang" trough during late Middle Permian and its petroleum geological significance in northern Sichuan Basin, SW China. Petrol. Explor. Dev. 48, 1–13 (in Chinese with English abstract).

Wang, Y.G., Chen, S.J., Xu, S.Q., 2001. The Formation Condition and the Prospecting Technology of the Gas Reservoir in Paleozoic and Upper Proterozoic in Sichuan Basin. Petroleum Industry Press, Beijing, pp. 67–78.

Wang, Y.G., Du, L.R., Wen, Y.C., Zhang, J., Liu, H.Y., 2002. Origin of H_2S in Triassic Feixianguan formation gas pools, northeastern Sichuan Basin, China. Geochimica 31, 517–524 (in Chinese).

Worden, R.H., Smalley, P.C., Oxtoby, N.H., 1995. Gas souring by thermochemical sulfate reduction at 140°C. AAPG (Am. Assoc. Pet. Geol.) Bull. 79, 854–863. https://doi.org/10.1306/8D2B1BCE-171E-11D7-8645000102C1865D.

Worden, R.H., Smalley, P.C., 1996. H_2S-producing reactions in deep carbonate gas reservoirs: Khuff Formation Abu Dhabi. Chem. Geol. 133, 157–171. https://doi.org/10.1016/s0009-2541(96)00074-5.

Wu, X.Q., Liu, Q.Y., Liu, G.X., Ni, C.H., 2019. Genetic types of natural gas and gas-source correlation in different strata of the Yuanba gas field, Sichuan Basin, SW China. J. Asian Earth Sci. 181, 103906.

Zhai, G.M., 1989. Petroleum Geology of China, vol. 10. Petroleum Industry Press, Beijing, p. 516.

Zhang, X.F., 2009. The Reservoir Formation and Preservation of Lower Triassic Feixianguan Formation, Northeastern Sichuan Basin. Ph.D thesis, China University of Petroleum, Beijing, p. 176.

Zheng, R.C., Wen, H.G., Zheng, C., Luo, P., Li, G.J., Chen, S.C., 2009. Genesis of dolostone of the Feixianguan formation, lower Triassic in the NE Sichuan Basin: evidence from rock texture and strontium content and isotopic composition. Acta Petrol. Sin. 25, 2459–2468 (in Chinese with English abstract).

Zhu, G.Y., Zhang, S.C., Liang, Y.B., Dai, J.X., Li, J., 2005. Isotopic evidence of TSR origin for H_2S-rich gases in the Feixianguan formation northeastern Sichuan Basin. Sci. China Earth Sci. 48, 1960–1971.

Zhu, G.Y., Fei, A.G., Zhao, J., Li, C., 2014. Sulfur isotopic fractionation and mechanism for thermochemical sulfate reduction genetic H_2S. Acta Petrol. Sin. 30, 3772–3786.
Zhu, Y.M., Wang, J.B., Hao, F., Zou, H.Y., Cai, X.Y., 2008. Geochemical characteristics and origin of natural gases from Xuanhan area, eastern Sichuan. Chin. J. Geol. 43, 518–532 (in Chinese).
Zou, H.Y., Hao, F., Zhu, Y.M., Guo, T.L., Cai, X.Y., Li, P.P., Zhang, X.F., 2008. Source rocks for the giant Puguang gas field, Sichuan Basin: implication for petroleum exploration in marine sequences in South China. Acta Geol. Sin. 82, 477–486. https://doi.org/10.1111/j.1755-6724.2008.tb00598.x.